JOURNAL OF PETROLOGY | VOLUME 50 | NUMBER 11 | PAGES 2063–2094 | 2009 | doi:10.1093/petrology/egp069

In Situ U–Pb and Trace Element Analysis of Accessory Minerals in the Kiruna District, Norrbotten, Sweden: New Constraints on the Timing and Origin of Mineralization

M. P. SMITH[1]*, C. D. STOREY[1]†, T. E. JEFFRIES[2] AND C. RYAN[1]

[1]SCHOOL OF ENVIRONMENT AND TECHNOLOGY, UNIVERSITY OF BRIGHTON, COCKCROFT BUILDING, LEWES ROAD, BRIGHTON BN2 4GJ, UK

[2]DEPARTMENT OF MINERALOGY, THE NATURAL HISTORY MUSEUM, CROMWELL ROAD, LONDON SW7 5BD, UK

RECEIVED JULY 24, 2008; ACCEPTED SEPTEMBER 21, 2009
ADVANCE ACCESS PUBLICATION NOVEMBER 4, 2009

Northern Norrbotten, Sweden is a key part of Baltic Shield and provides a record of magmatic, tectonic and related, superimposed, Fe oxide–apatite and iron oxide–copper–gold (IOCG) mineralization, during the Svecokarelian orogeny. Titanite and allanite from a range of mineral deposits in the area have been analysed for U–Pb isotope systematics and trace element chemistry using laser ablation quadrupole inductively coupled plasma-mass spectrometry (LA-ICP-MS). Analyses of a single sample from the regional scapolite–albite alteration give an age of 1903 ± 8 Ma (2σ) and may be contemporaneous with the early stages of Fe mineralization (1890–1870 Ma). Analyses of titanite and allanite from undeformed IOCG deposits indicate initial alteration at 1862 ± 16 Ma. In many deposits subsequent metamorphic effects reset titanite isotope systematics from 1790 to 1800 Ma, resulting in a spread of U–Pb isotope analyses along concordia. In some instances core regions may record evidence of early thermal events at around 2050 Ma. Titanite and allanite from deformed IOCG deposits on major shear zones record ages from 1785 ± 21 Ma to 1777 ± 20 Ma, corresponding to deformation, metamorphism and secondary hydrothermal alteration as a result of late orogenic movements. The lack of intracrystalline variations in titanite and allanite trace element chemistry suggests that hydrothermal fluid chemistry and metal source were the main controls on mineral trace element chemistry. Titanite from undeformed Fe oxide–apatite and IOCG deposits is typically light rare earth element (LREE) enriched, and shows low U/Th ratios and low Ni in both intermediate to acid and basic volcanic-hosted deposits. This is consistent with a granitic source for metals. Minor variations in trace element patterns are consistent with the influence of aqueous complex formation on relative REE solubility. Deposits related to the Nautanen Deformation Zone have relatively heavy REE (HREE)-enriched titanite, and LREE-depleted allanite, with high U/Th ratios and elevated Ni contents, consistent with leaching of metals from the local basic volcanic rocks. All hydrothermal titanites are high field strength element enriched (Nb, Ta, Zr) indicating their transport as a result of either high salinities or high F contents, or both. The data overall support models of IOCG-type mineralization as a result of regional circulation of saline hydrothermal fluids in association with major crustal structures, with at least some metallic components derived from the granitoid rocks of the area. All the deposits here show evidence of subsequent metamorphism, although penetrative fabrics are restricted to regional-scale deformation zones.

KEY WORDS: *allanite; IOCG; Kiruna; titanite; U–Pb geochronology*

INTRODUCTION

The iron oxide–copper–gold (IOCG) family of deposits, originally proposed by Hitzman *et al.* (1992), has been the focus of intense investigation in recent years, in terms of defining both genetic (e.g. Barton & Johnson, 1996, 2000;

*Corresponding author. Telephone: +44 (0) 1273 642265. Fax: +44 (0) 1273 642285. E-mail: martin.smith@brighton.ac.uk
†Present address: Department of Earth Sciences, University of Bristol, Wills Memorial Building, Queen's Road, Bristol BS8 1RJ, UK

Pollard, 2006) and exploration models (e.g. Smith, 2002). The original definition of the deposit type included deposits dominated by iron oxides with accessory apatite, as well as those with significant Cu mineralization, and led to comparisons with deposits as wide-ranging as porphyry coppers, carbonatites and sedimentary hosted Cu ores. More recent reviews have tried to rationalize the definition (Hitzman, 2000; Williams *et al.*, 2005). Williams *et al.* (2005) proposed as criteria the presence of Cu with or without Au as economic metals, hydrothermal vein, breccia and/or replacement ore styles, characteristically in specific structural sites, abundant magnetite and/or hematite, low Ti contents in iron oxides relative to those in most igneous rocks and the absence of clear spatial associations with igneous intrusions. Common features, not always present, also listed by Williams *et al.* (2005) included crustal settings with exceptionally voluminous, generally pervasive, alkali metasomatism, and a suite of minor elements including F, P, Co, Ni, As, Mo, Ag, Ba, light rare earth elements (LREE) and U. Shallower systems may show sericitic and carbonate alteration alongside widespread hematite (e.g. Olympic Dam). This review paper also definitively stated that Kiruna-type Fe-oxide deposits and Fe skarns are not IOCG deposits, but share many characteristics and may be linked. Recent work has suggested a significant difference in the timing of the two deposit types (Hitzman, 2000); however, the early stage magnetite alteration in many IOCG deposits, the late-stage occurrence of pyrite, chalcopyrite and gold in and near massive magnetite deposits, and the common alteration features associated with both deposit types still support a link (Sillitoe, 2003). The overall genetic mechanisms of the deposits remain a subject of debate, with current models ranging from the circulation of brines derived from calc-alkaline magmas along major tectonic structures (Pollard, 2006), to mineralization related to the circulation of fluids derived either from the dissolution of evaporites or from continental surface brines (Barton & Johnson, 1996, 2000). Williams *et al.* (2005) concluded that a range of processes may give rise to the common characteristics, and that a range of sources may contribute hydrothermal fluid components in different settings, and therefore more research is needed before it can be concluded that either a single genetic mechanism, or a range of mechanisms in different geological environments lead to the formation of deposits with common characteristics.

The Kiruna district in Sweden is the type area for Fe oxide–apatite deposits, and hosts a number of actively or historically mined deposits that have been linked to the IOCG class. Geochronological data from the area have not yet fully distinguished the IOCG and magnetite–apatite deposits in time, and major debates remain about the genetic mechanism of both deposit types. Equally, the complex geological history of the district means that bulk grain analytical techniques for phases such as zircon and titanite do not adequately distinguish the multiple thermal events that have affected rocks from the area (Storey *et al.*, 2007). Here we present an *in situ* study of the U–Pb isotope systematics and trace element chemistry of titanite and allanite from a range of deposits, carried out using laser-ablation inductively coupled plasma-mass spectrometry (LA-ICP-MS). Despite the lower precision of this technique compared with isotope dilution thermal ionization mass spectrometry (ID-TIMS), the increased spatial resolution and capability for *in situ* analyses of texturally characterized grains (Storey *et al.*, 2006, 2007) means that this technique is ideal for application in mineral deposits with complex post-mineralization histories. The deposits sampled cover a significant range in structural setting, but similarities in alteration style, and hence potential genetic mechanisms, indicate that it is pertinent to examine the deposits together.

BACKGROUND GEOLOGY

The major iron ore province of northern Sweden is hosted within Palaeoproterozoic rocks, mainly Karelian (2·5–2·0 Ga) and Svecofennian (1·9–1·88 Ga) in age, which extend from northern Sweden into Finland and parts of northern Norway (Fig. 1). The geology and metallogeny of the Norrbotten area have recently been reviewed by Carlon (2000) and Bergman *et al.* (2001). The Palaeoproterozoic rocks of the area were deposited between 2·5 and 1·85 Ga and are now preserved in deformed metamorphic belts, intruded by a range of granitoid plutons. The Greenstone Group (>1·9 Ga) consists of tholeiitic to komatiitic volcanic rocks (Ekdahl, 1993; Martinsson, 1997) and is overlain first by the Middle Sediment Group (Witschard, 1984), then by the dominantly andesitic Porphyrite Group, which consists of volcanic and sub-volcanic rocks, and then by the Kiirunavaara Group (Martinsson, 2004). The Kiirunavaara Group consists of syenitic and quartz-syenitic igneous rocks and intercalated sediments, which host the Kiirunavaara magnetite–apatite deposit. The syenitic character of these rocks may be the result of alteration overprinting an original calc-alkaline signature. The Haparanda and Perthite calc-alkaline and alkali–calcic monzonite granite suites intruded these rocks between 1·9 and 1·8 Ga (Skiöld, 1987) followed by the Lina suite granitoids at around 1·79 Ga (Skiöld, 1988; Bergman *et al.*, 2001). A period of deformation and metamorphism of the supracrustal sequence accompanied the intrusion of these granitoids, with conditions peaking at upper greenschist or lower amphibolite facies (Bergman *et al.*, 2001). The youngest plutonic rocks in the area are TIB 2 granitoids, at around 1·71 Ga in age, exposed at the Swedish–Norwegian border (Romer *et al.*, 1992).

The volcanic sequence is affected by scapolitization and albitization at both the regional and deposit scale,

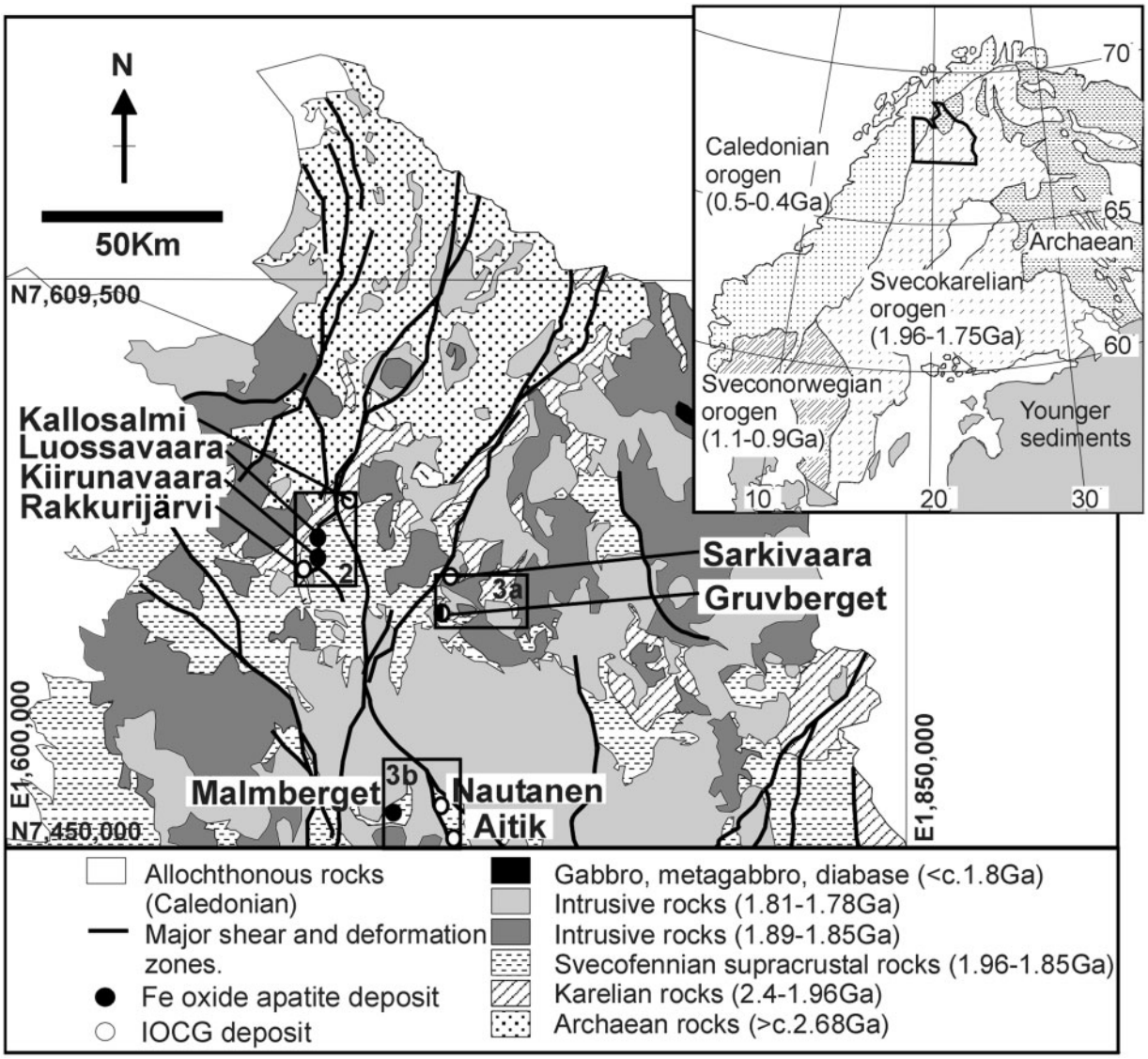

Fig. 1. Simplified geological map of northern Norrbotten county, Sweden, showing the location of the mineral deposits and prospects studied. Main map coordinates refer to Swedish National Grid (RT90). Rectangles show locations for Figs 2 and 3. Adapted from Bergman *et al.* (2001).

in association with both iron oxide and Cu–(Au) mineralization (Frietsch *et al.*, 1997). The Fe oxide–apatite bodies are typified by the Kiirunavaara–Luossavaara body, dominated by magnetite, and the Per Geiger ores, with both hematite and magnetite (Geijer, 1910, 1931; Martinsson, 2004). The deposits are accompanied by sodic and potassic alteration (albite–K-feldspar–biotite), in some instances including scapolite. Potassic alteration typically overprints sodic alteration, but multiple events do occur in some deposits (e.g. Rakkurijärvi, Smith *et al.*, 2007). The IOCG-type deposits occur both as relatively undeformed bodies hosted by the Greenstone, Porphyrite and Kiirunavaara Groups (e.g. Pahtohavare; Lindblom *et al.*, 1996) and as strongly deformed bodies associated with major deformation zones [e.g. Nautanen and Aitik on the Nautanen Deformation Zone (NDZ); Martinsson & Wanhainen, 2004]. Chalcopyrite mineralization is typically spatially associated with early magnetite and scapolite–albite alteration and later potassic and finally carbonate alteration, although major Cu-mineralization is typically later than the development of magnetite. The NDZ is a NNW-trending tectonic structure in which strongly schistose or mylonitic rocks occur in several high-strain branches in a zone up to 3 km wide. The Nautanen deposit is hosted in sheared quartz veins associated with K-feldspar–epidote alteration, scapolitization, tourmalinization, sericitization and the development of metasomatic garnet (Martinsson & Wanhainen, 2004).

The samples used in this study are described in Table 1 and the sample site geology is shown in Figs 2 and 3. The sites include Fe oxide–apatite bodies (Kiirunavaara–Luossavaara; Malmberget; Gruvberget), relatively undeformed IOCG deposits [Rakkurijärvi (Smith *et al.*, 2007); Kallosalmi (Wägman & Ohlsson; 2000); Gruvberget (Martinsson & Virrkunen, 2004)] and deposits hosted by the NDZ. Samples were also taken from massive scapolite skarn-hosted Cu–Mo mineralization at Sarkivaara (Wägman & Ohlsson, 2000), and from the footwall sodic altered granodiorite at the actively mined Cu–Au deposit at Aitik (Wanhainen *et al.*, 2003). These samples both had very low U concentration and high $^{206}Pb/^{204}Pb$ contents, and so did not yield reliable U–Pb ages but are included for their trace element data. U–Pb isotope and REE compositional data from samples from Luossavaara, Malmberget and Gruvberget were previously reported by Storey *et al.* (2007); here we present an expanded range of trace element analyses and compare these samples with those from other deposit types.

METHODS

Rock samples were cut into polished sections *c.* 150 μm thick revealing large crystals of titanite exposed at the surface. These were studied optically and as uncoated specimens using a JEOL 5900LV scanning electron microscope (SEM) at the Natural History Museum, London (NHM) operating at low vacuum conditions to minimize charging effects. U–Pb isotope analyses were then undertaken by LA-ICP-MS at the NHM. Samples were then very lightly polished and cleaned to removed excavated material from the vicinity of laser ablation (LA) pits, then carbon coated for electron microprobe analysis (EMPA). This was done after the U–Pb analyses to ensure that the coating process did not add contamination to sample surfaces. EMPA sites were made as close as possible to the U–Pb LA pits. After this the coating was carefully removed for trace element analysis by LA-ICP-MS, which was performed at each EMPA site. Samples were finally gently polished and cleaned before being re-coated for further high-quality electron imaging.

U–Pb isotope analysis

Sample surfaces were cleaned by rinsing with dilute (*c.* 5%) HNO_3 and deionized water. Once fully dry, the samples were mounted in a specially adapted laser cell for thick sections, and loaded into a NuWave UP213 Nd:YAG laser ($\lambda = 213$ nm) port, linked to a PlasmaQuad 3 quadrupole ICP-MS system (Storey *et al.*, 2006). Operating conditions are listed in Table 2. Laser beam diameter and line scan length are listed for each analysis in Table 3 and Electronic Appendix 1, which is available for downloading at http://www.petrology.oxfordjournals.org/. Line raster scans were performed within areas of distinct backscattered electron (BSE) image contrast. Normalization to zircon geostandard 91500 (Wiedenbeck *et al.*, 1995) and age calculation were performed off-line using the macro spreadsheet-based procedure LAMTRACE, developed by S. Jackson of Macquarie University, Australia. Storey *et al.* (2006) demonstrated that when using rastered lines matrix matching was not a prerequisite for precise and accurate U–Pb analyses of titanite. Plotting of U–Pb data was performed using ISOPLOT v. 3 (Ludwig, 2003). The time-resolved plot of Pb/Pb and Pb/U ratios from each analysis was studied and only analyses, or coherent parts of analyses, that showed no mixed age data, secondary phases or potentially contaminated fractures encountered during analysis were chosen for final age calculation. All analyses were corrected for common Pb by measurement of the ^{204}Pb isotope, corrected for isobaric interference from Hg aided by the use of inline gold traps on the carrier gas lines (Storey *et al.*, 2006). Pb/U ratios were corrected using model terrestrial Pb composition values (Stacey & Kramers, 1975) at the age of crystallization.

The main measured ratio contributing to discordance after applying a ^{204}Pb common Pb correction was the $^{207}Pb/^{235}U$ ratio. This is due to the much lower concentration of these isotopes. In this study we chose to propagate measured uncertainty from only the $^{201}Hg/^{204}Hg(Pb)$ onto the $^{207}Pb/^{235}U$ uncertainty and not the more precisely measured $^{206}Pb/^{238}U$ ratio. The result in nearly all cases is that the error ellipses overlap concordia, implying that all relevant sources of uncertainty have been taken into account. We report the age based on the $^{206}Pb/^{238}U$ ratio corrected for common Pb based on these factors, apart from where discussed separately below. Pb/U and Pb/Pb isotopic data are presented in Table 3 alongside common Pb-corrected ages based on the $^{207}Pb/^{206}Pb$ mathematical approach (Williams, 1998) for comparison with ^{204}Pb corrected ages. The full dataset is available in Electronic Appendix 1.

SEM characterization and electron microprobe analysis

Following LA-ICP-MS U–Pb isotope analysis, samples were carbon coated and examined using the backscattered electron (BSE) mode of a JEOL 6310 SEM at the University of Brighton to accurately locate the ablation sites. The titanites were then chemically analysed using a Cameca SX50 electron microprobe housed at the NHM. Run conditions were 15 kV accelerating voltage and a beam current of 20 nA. The instrument was calibrated using natural mineral and pure material standards including perovskite for Ca and Ti, jadeite for Na, wollastonite for Si, corundum for Al, monazite for Th, synthetic oxides for Fe, Mg and U, pure metals for Ta, Mn, and Nb, and a range of synthetic single REE-bearing glasses (prepared by P. Hill, Edinburgh). Element–element interferences for

Table 1: Sample localities and descriptions

Area	Sample number	Depth (m)	Host group	Grid reference*		Sample description	Titanite/allanite textural setting
				Northing	Easting		
Regional sodic alteration							
Nunasvaara	03NUN30		Greenstone Group	7523895	1738674	Brecciated scapolitized metadiorite/metagabbro	1 cm titanite in scapolitized amphibolite
Fe oxide–apatite deposits							
Luossavaara	03LUOSS01†		Kiirunavaara Group	7538040	1685606	Magnetite–titanite veined and altered syenite porphyry	0·5 cm titanite in amygdales with magnetite, actinolite, calcite and albite
Kiirunavaara	KR1		Kiirunavaara Group	7534260	1684610	Porphyry breccia with actinolite–hematite–quartz–calcite cement	0·5 cm titanite in breccia cement
Gruvberget	03GRUV22†		Porphyrite Group	7515145	1719960	Potassic (epidote–actinolite–K-feldspar) altered metavolcanic rock	1 cm titanite nucleated on rutile in quartz–actinolite–albite–magnetite altered rock
Malmberget	03VALK01†		Kiirunavaara Group	7462074	1708551	Actinolite–feldspar–quartz vein cutting potassic altered metavolcanic rock	1 cm titanite in vein with apatite, magnetite, minor hematite
Cu–(Au) deposits							
Sarkivaara	SAR1		Porphyrite Group	7519320	1719946	Scapolite–actinolite–epidote skarn with chalopyrite and molybdenite	Up to 2 mm titanite associated with scapolite and epidote–sulphide veinlets
Rakkurijärvi	01 RAK 006	183·0	Kiirunavaara Group	7526507	1682450	Potassic alteration overprinting scapolitization in meta-trachyandesite	Titanite and allanite in clots associated with apatite and biotite
Kallosalmi	KAL 90107	56·4	Greenstone Group	7542113	1692714	Scapolite–actinolite altered metabasalt with overprinting carbonatization	Titanite occurs throughout the altered rock matrix
Aitik	A3		Porphyrite Group (N‡)	7540620	1687050	Actinolite vein with albitization and epidotization in footwall granodiorite	Titanite in actinolite–albite altered granodiorite
Nautanen	NAU 84012	159·9	Porphyrite Group (N‡)	7463871	1719900	Well-foliated epidote–actinolite–albite schist with coarse titanite	1–2 mm titanite aligned with schistosity, allanite as zones and cores in epidote
Nautanen	NAU 77006	164·4	Porphyrite Group (N‡)	7463947	1719762	Scapolite–actinolite–albite schist with epidote overprint	Titanite associated with scapolite–actinolite alteration

*Swedish national grid (RT90) reference.
†Sample U–Pb and REE analyses reported by Storey *et al.* (2007).
‡N, Associated with the Nautanen Deformation Zone (NDZ).

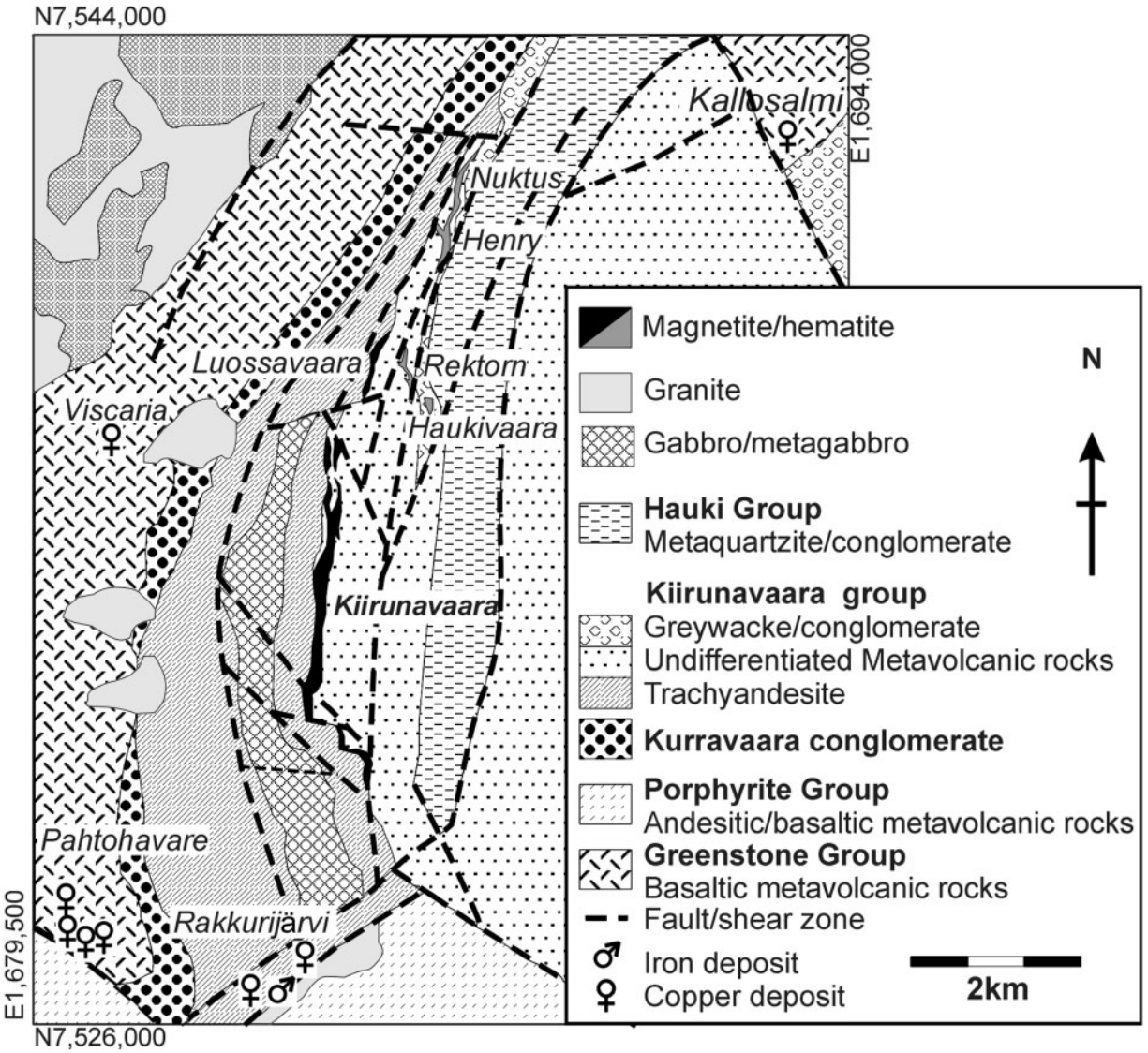

Fig. 2. Geological map of the Kiruna area showing the locality of the mineral deposits studied, and other deposits mentioned in the text. Map coordinates refer to Swedish National Grid (RT90). Adapted from Sveriges Geologiska Undersökning (1967), Martinsson & Wanhainen (2000) and Bergman *et al.* (2001).

the REE were corrected using analyses of these glasses and the method outlined by Williams (1996). A second set of analyses was also run including F and using topaz as a standard. Results are shown in Tables 4 and 5.

Trace element analysis

Trace element analyses of titanite and allanite were carried out using the same analytical equipment as that for U–Pb analysis, except that the in-line Au traps were removed. All analyses used NIST 612 glass as an external standard, and used Ca determined by electron microprobe as an internal standard to convert element ratios to absolute concentrations. The 1σ precision on NIST 612 glass from this study is typically around 2–4%. Accuracy was monitored using a glass prepared from Colombia River Basalt (USGS sample BCR-2G). The results are compared with accepted values for BCR-2 rock powder and previous analyses of BCR-2G in Table 6. Our results are within error of the accepted values for BCR-2 or within the published range of analyses of BCR-2G (Jochum *et al.*, 2005) for most elements. Our values are significantly different for Mn, U, Ti, Mo and Sr, but it has been noted that the glass has heterogeneities for some elements (notably Mo) introduced by the glass preparation procedure (Norman *et al.*, 1998). The cross-comparison between glass secondary standards and minerals is valid as numerous studies have

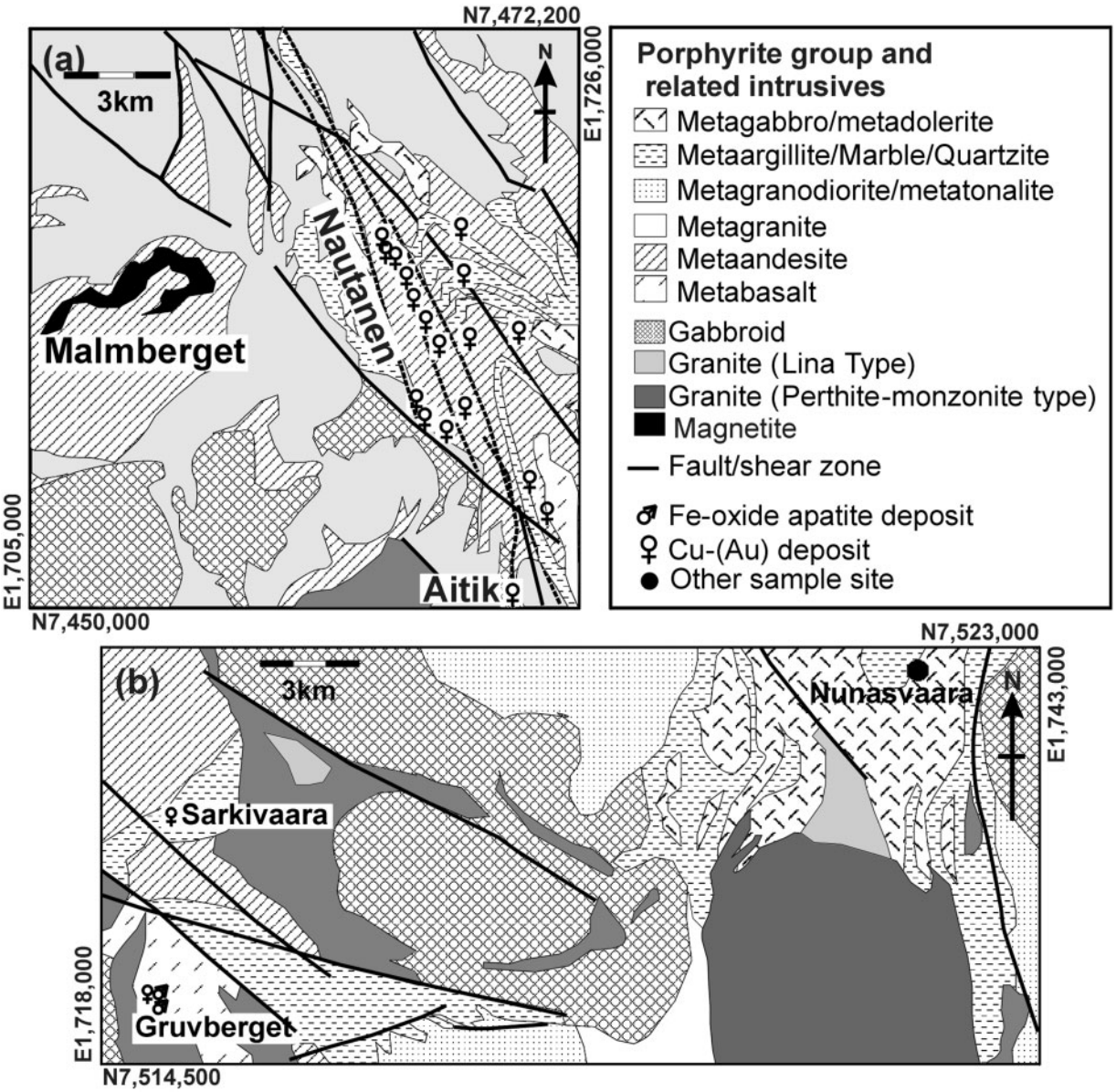

Fig. 3. (a) Geological map of the Malmberget–Nautanen area showing the locality of the mineral deposits studied. (b) Geological map of the Gruvberget area showing the locality of the deposits studied and other sample sites. Map coordinates refer to Swedish National Grid (RT90). Adapted from Bergman *et al.* (2001).

shown that matrix matching is not necessary for precise and accurate standardization of LA-ICP-MS trace element analyses (Jeffries, 2004). We are therefore confident that our analyses reflect both relative and absolute variation in trace element concentrations in titanite.

RESULTS

U–Pb geochronology of titanite and allanite

U–Pb isotopic data from morphologically complex titanite grains from Luossavaara, Gruvberget and the Valkommen body at Malmberget have previously been discussed by Storey *et al.* (2007). BSE imaging of these titanites revealed low mean atomic number (Z) cores and high mean Z overgrowths. REE analyses indicated in two out of three samples that the core and rim zones are distinct and support a model for two-stage growth. *In situ* U–Pb analysis reveals that the titanite cores in all three samples retain distinct older ages of *c.* 2050 Ma, whereas the rims have either distinct younger or strongly reset ages. The older cores were interpreted as representing the first alteration or metamorphism of the volcanic pile. In the case of the rims,

Table 2: Machine conditions and protocols for LA-ICP-MS U–Pb and trace element analyses

Laser parameters	
Laser	NewWave Research UP213
Wavelength	213 nm
Pulse width	3 ns
Energy distribution	Homogenized, flat beam, aperture
Pulse energy	0·01–0·1 mJ per pulse
Energy density	4 J/cm^2
Focus	Fixed at surface
Repetition rate	20 Hz
Raster scan speed	10 μm/s
Nominal spot diameter	30–60 μm (unknowns), 60 μm (standard)

ICP-MS parameters	
ICP-MS system	Thermo Elemental PlasmaQuad 3 with 'Soption'
Forward power	1350 W
Gas flows	
Coolant (plasma) Ar	13 l/min
Auxiliary Ar	0·8 l/min
Sample transport He	*c*. 1·1 l/min
Sample transport Ar	*c*. 0·9 l/min
Analysis protocol	
Scanning mode	Peak hopping, 1 point/peak
Acquisition mode	Time-resolved analysis
Analysis duration	180 s (*c*. 60 s background, 120 s signal)
Dwell times	
^{201}Hg, ^{204}Hg/Pb	10 ms
^{206}Pb, ^{208}Pb, ^{232}Th, ^{238}U, ^{207}Pb, ^{235}U	30 ms

a sample from Luossavaara records a U–Pb age of 1870 ± 24 Ma (2σ), whereas in a sample from Gruvberget the rims record a U–Pb age of 1820 ± 10 Ma (2σ), consistent with previous studies (Romer *et al*., 1994). In the sample from Malmberget U–Pb ages spread along concordia from *c*. 1920 to 1708 Ma, attributed to metamorphic rehomogenization of primary metasomatic titanite in accordance with the strong deformation and metamorphism of the deposit.

For the new data presented here a number of samples display a spread of analyses along concordia, and in one instance record discordant ages. We have utilized cumulative probability plots based on ^{206}Pb/^{238}U ages to identify normally distributed ages, where a weighted mean of analyses may have real significance, and samples where there is significant spread along concordia to identify peaks in the probability distribution. Lead loss as a result of subsequent metamorphism or weathering may explain this; however, the textures in many examples, including cores with infilled microporosity at the junction with the rim (Fig. 4a), BSE light core remnants with darker overgrowths and fracture fills (Fig. 4b) and chemically homogenous, porous grains, strongly indicate that coupled dissolution–reprecipitation (Putnis, 2002) is the most likely and kinetically favourable mechanism for chemical and isotopic rehomogenization of titanite. Indicative textures of this recrystallization mechanism have now been reported from zircon in a number of settings (e.g. Tomaschek *et al*., 2003). Because of this we interpret multiple peaks in most cumulative probability plots as indicating discrete events rather than continuous diffusive lead loss.

Greenstone Group diorite samples from the Nunasvaara area are scapolitized and brecciated, with large amounts of actinolite forming the matrix and locally large crystals of titanite (Table 1). BSE imaging of one grain *c*. 1 cm in diameter revealed that it comprises BSE dark areas overprinted by BSE lighter areas around grain rims and along fractures. The dark areas have lower U concentrations and higher ^{207}Pb/^{206}Pb ratios, and the light areas provide a group of concordant (or near concordant) homogeneous ages (Table 3, Fig. 5). The analyses from the BSE dark areas did not result in reliable ages and are omitted here. The whole crystal appears to have undergone some degree of recent Pb loss resulting in discordance, and so the rim analyses are regressed through 0 Ma. The result is a well-constrained age of 1903 ± 8 Ma from the young group of BSE bright analyses.

Sample KR1 was taken from the hanging wall to the main magnetite–apatite mineralization at Kiirunavaara (Table 1), where titanite with a grain size up to 1 mm in diameter occurs in the quartz–calcite matrix of a metavolcanic breccia. Of 24 analyses, 22 had detectable amounts of common Pb (Table 3). Corrected analyses overlap concordia (Fig. 6b) and spread from *c*. 1850 to 1750 Ma with a weighted mean age of 1801 ± 25 Ma (95% confidence). The spread along concordia could be attributed to either minor Pb loss or a later thermal event. A bimodal distribution of single ^{206}Pb/^{238}U ages indicates this mean does not represent a possible age. The older age (1894 ± 35 Ma) along this spectrum is within error of the calculated age for Fe oxide–apatite mineralization in the footwall to the Luossavaara deposit a few kilometres along strike from KR1 of 1870 ± 24 Ma (Storey *et al*, 2007; Table 3), as is the initial cumulative probability peak at 1860 Ma. Because of the well-preserved zonation, and hence lack of textural evidence for recrystallization by dissolution–reprecipitation (Putnis, 2002), it is considered likely that titanite began to crystallize during mineralization at Kiirunavaara and underwent a later thermal resetting event at *c*. 1780 Ma where there is a second mode in the cumulative probability plot.

Table 3: Representative corrected U–Pb isotope ratios and calculated ages

	Analysis number	Mineral	Beam diameter (μm)	Line length (μm)	Corrected isotope ratios and errors (%)*							Ages (Ma)			
					$^{206}Pb/^{204}Pb$	$^{207}Pb/^{235}U$	±2σ	$^{206}Pb/^{238}U$	±2σ	$^{207}Pb/^{206}Pb$	±2σ	^{204}Pb corrected†		$^{207}Pb/^{206}Pb$ corrected‡	
												$^{206}Pb/^{238}U$	±2σ	$^{206}Pb/^{238}U$	±2σ
03NUN30	mr31a09	t	60	55	2743	4·381	14·40	0·330	2·03	0·112	14·31	1840	*38*	1842	36
	mr31a14	t	60	45	b.d.							*1912*	*81*	1914	80
	mr31a16	t	45	60	1002	4·002	9·81	0·325	3·68	0·105	9·18	1837	68	1826	66
01RAK006	au25b05	a	60	82	2257	6·347	20·92	0·344	2·99	0·136	20·75	1905	57	1865	56
	au25b09	a	60	70	3466	5·097	20·94	0·329	1·83	0·114	20·94	1835	34	1832	33
	au25b16	a	60	67	1735	5·284	20·33	0·342	1·93	0·114	20·33	1896	37	1900	37
	au25a14	t	60	49	433	4·546	18·72	0·311	2·40	0·109	18·54	1744	42	1740	41
	au25b11	t	60	61	479	5·077	18·74	0·325	1·92	0·114	18·66	1812	35	1806	36
	au25b12	t	60	66	823	5·751	1·83	0·340	2·10	0·128	20·52	1885	40	1859	40
NAU84012	au26a05	t	45	70	4813	4·525	15·76	0·318	2·17	0·105	15·66	1719	24	1786	38
	au26a07	t	45	64	10137	4·581	10·53	0·313	1·65	0·108	10·49	1768	31	1755	29
	au26a09	t	45	66	2183	4·434	17·29	0·305	3·03	0·107	17·05	1749	20	1712	51
	au26a14	a	45	60	5·028	4·876	18·57	0·325	2·57	0·111	18·47	1819	27	1815	46
	au26a15	a	45	72	5·072	4·597	12·56	0·314	3·25	0·108	12·33	1765	30	1758	56
	au26a16	a	45	58	5·396	3·979	12·25	0·313	3·15	0·095	11·77	1753	55	1775	28
NAU77006	au27a08	t	30	48	b.d.							*1731*	*42*	1721	41
	au27a10	t	30	50	1007	4·201	16·21	0·316	2·36	0·100	16·11	1771	42	1787	41
	au27a11	t	30	45	2972	4·690	16·50	0·332	2·39	0·107	16·53	1847	44	1859	44
KR1	au23a10	t	60	74	1311	4·514	14·35	0·312	2·36	0·110	14·32	1749	43	1739	40
	au23a11	t	60	70	374	5·098	13·29	0·337	1·98	0·117	13·19	1874	44	1877	37
	au23a12	t	60	57	415	4·834	15·64	0·321	2·12	0·113	15·55	1795	43	1761	37
KAL90107	au24b05	t, b	45	60	b.d.							*1741*	*30*	1729	15
	au24b06	t, d	45	63	b.d.							*1961*	*37*	1944	19
	au24b12	t, b	45	63	b.d.							*1852*	*31*	1858	15
	au24c06	t, i	45	61	b.d.							*1826*	*79*	1822	38

The full dataset and uncorrected isotope ratios are given in Electronic Appendix 1. a, allanite; t, titanite; b, BSE bright; d, BSE dark; i, BSE intermediate.
*Corrected for common Pb (^{204}Pb method), blank means $^{206}Pb/^{204}Pb$ below detection, so $^{207}Pb/^{206}Pb$ corrected age should be used.
†^{204}Pb corrected $^{206}Pb/^{238}U$ age. Errors quoted are propagated only through the reproducibility of the standard. Where ^{204}Pb is below detection, the uncorrected $^{206}Pb/^{238}U$ age is quoted and shown in italics.
‡Corrected using the mathematical approach of Williams (1998).

Table 4: Representative electron microprobe analyse of titanite

	Detection limit	Nunasvaara		Luossavaara		Kiirunavaara		Gruvberget		Malmberget		Sarkivaara		Kalosalmi	Nautanen	
				Core	Rim			Core	Rim							
Na_2O	0·02	0·03	0·03	0·03	0·07	0·09	0·05	0·03	0·04	0·00	0·08	0·03	0·02	0·02	0·01	0·08
CaO	0·01	28·0	27·6	27·3	27·7	26·9	27·1	27·9	27·5	28·00	26·2	27·4	28·1	27·8	27·9	27·4
MgO	0·02	b.d.	b.d.	b.d.	0·03	0·03	0·06	b.d.	b.d.	b.d.	b.d.	b.d.	b.d.	b.d.	b.d.	b.d.
MnO	0·02	0·04	b.d.	0·02	b.d.	0·04	0·03	0·09	0·05	0·14	0·02	0·07	0·03	0·04	0·23	0·17
Fe_2O_3	0·02	0·56	1·26	1·15	2·08	2·05	2·62	0·58	1·02	0·84	2·52	0·72	1·98	0·13	0·84	1·41
TiO_2	0·11	38·9	37·7	37·9	37·0	36·5	36·0	39·1	37·3	38·1	36·0	38·6	33·3	39·0	38·2	35·7
La_2O_3	0·12	b.d.	0·15	b.d.	0·13	0·21	0·12	b.d.	b.d.	b.d.	0·13	b.d.	b.d.	b.d.	b.d.	b.d.
Ce_2O_3	0·11	0·35	0·72	0·91	0·52	0·81	0·55	0·34	0·34	0·19	1·11	0·25	0·14	0·53	0·15	0·17
Nd_2O_3	0·09	0·09	0·24	0·43	b.d.	0·22	0·12	b.d.	0·17	b.d.	0·59	b.d.	b.d.	0·27	b.d.	b.d.
SiO_2	0·03	30·2	30·1	30·1	30·1	30·1	30·3	30·3	30·7	30·3	29·5	30·7	30·7	30·3	30·2	30·0
Al_2O_3	0·01	0·46	0·76	0·59	0·65	0·49	0·74	0·35	0·82	0·90	0·88	0·62	3·19	0·58	0·96	1·56
F	0·02	n.a.	n.a.	b.d.	0·09	0·13	0·26	b.d.	b.d.	b.d.	b.d.	b.d.	b.d.	b.d.	b.d.	b.d.
H_2O*		0·001	0·003	0·002	0·003	0·003	0·003	0·001	0·003	0·002	0·005	0·002	0·008	0·001	0·003	0·004
Total		98·7	98·8	98·6	98·5	97·7	97·9	98·7	98·0	99·1	97·4	98·3	97·5	98·6	99·0	96·8
O = F				0·00	0·04	0·05	0·11	0·00	0·00	0·00	0·00	0·00	0·00	0·00	0·00	0·00
Total		98·7	98·8	98·6	98·4	97·7	97·8	98·7	98·0	99·1	97·4	98·3	97·5	98·6	99·0	96·8
Formulae to 20 (O, OH, F)																
Na		0·007	0·007	0·007	0·018	0·025	0·014	0·008	0·009	0·001	0·021	0·007	0·005	0·004	0·001	0·021
Ca		3·981	3·945	3·904	3·969	3·893	3·894	3·960	3·927	3·943	3·825	3·893	4·022	3·952	3·956	3·965
Mg					0·005	0·007	0·012									
Mn		0·004		0·002	0·002	0·004	0·003	0·010	0·006	0·020	0·003	0·008	0·003	0·004	0·025	0·019
Fe		0·056	0·126	0·116	0·209	0·208	0·264	0·058	0·103	0·083	0·257	0·072	0·199	0·013	0·084	0·143
Ti		3·882	3·781	3·806	3·723	3·707	3·641	3·898	3·744	3·769	3·681	3·845	3·351	3·893	3·804	3·627
La			0·007		0·006	0·011	0·006				0·007					
Ce		0·017	0·035	0·045	0·026	0·040	0·027	0·016	0·016	0·010	0·055	0·012	0·007	0·026	0·007	0·008
Nd		0·004	0·011	0·020		0·011	0·006		0·008		0·029			0·013		
Si		4·007	4·011	4·017	4·020	4·060	4·075	4·017	4·091	4·058	4·018	4·065	4·100	4·021	3·998	4·061
Al		0·071	0·120	0·093	0·102	0·078	0·117	0·054	0·129	0·132	0·141	0·096	0·503	0·091	0·149	0·248
F				0·000	0·038	0·055	0·111									
OH*		0·128	0·246	0·208	0·273	0·231	0·270	0·113	0·232	0·215	0·399	0·168	0·702	0·103	0·233	0·391

b.d., below detection; n.a., not analysed.
*Estimated from charge balance.

Table 5: Representative electron microprobe analyses of allanite

	Detection limit	Rakkurijärvi 01RAK006		Nautanen NAU84012	
Na_2O	0·02	0·01	0·00	0·05	0·01
CaO	0·01	12·4	13·7	18·9	20·3
MgO	0·02	0·91	0·47	0·26	0·21
MnO	0·02	0·13	0·13	0·54	0·33
Fe_2O_3	0·02	15·7	16·3	13·6	13·8
TiO_2	0·11	0·68	0·39	0·07	0·10
La_2O_3	0·12	10·1	8·7	2·6	2·0
Ce_2O_3	0·11	9·5	7·9	3·4	2·2
Pr_2O_3	0·09	0·69	0·60	0·43	0·33
Nd_2O_3	0·09	0·84	0·80	1·36	0·87
SiO_2	0·03	31·8	32·3	35·1	36·1
Al_2O_3	0·01	14·9	15·6	20·3	21·6
H_2O^*		1·6	1·7	1·8	1·9
Total		99·4	98·7	98·7	99·8
Formula to 13 (O, OH)					
Na		0·002	0·000	0·008	0·002
Ca		1·213	1·325	1·722	1·795
Mg		0·124	0·064	0·032	0·026
Mn		0·010	0·010	0·039	0·023
Fe		1·072	1·105	0·870	0·858
Ti		0·185	0·106	0·018	0·026
La		0·338	0·289	0·081	0·062
Ce		0·315	0·263	0·106	0·066
Pr		0·158	0·135	0·013	0·010
Nd		0·027	0·026	0·041	0·026
Si		2·893	2·916	2·985	2·977
Al		1·603	1·655	2·035	2·099

*H_2O calculated assuming a full hydroxyl site occupancy.

Titanite and allanite were analysed from an altered trachyandesite from the Rakkurijärvi Cu–Au prospect (Table 1; Smith *et al.*, 2007). The sample shows early albitization (sodic alteration) overprinted by subsequent K-feldspar–scapolite (sodic–potassic) alteration (Smith *et al.*, 2007). Sample 01 RAK 006 183.2m contains oscillatory zoned, subhedral allanite grains *c.* 500 μm in diameter, and small, euhedral titanite grains *c.* 100 μm in diameter. In all, 24 analyses were made, 18 on allanite and six on titanite, using a beam diameter of 60 μm. Most of the analyses are slightly to moderately discordant, and lie on a mixing line between the age on U–Pb concordia and the common Pb composition. Allanite ^{204}Pb-corrected data straddle the concordia (Fig. 7c) and give a well-defined unimodal probability peak (Fig. 7d). All ^{204}Pb-corrected ^{206}Pb/^{238}U ages have a weighted average age of 1854 ± 18 Ma (95% confidence; Fig. 7c), compared with a weighted average of ^{207}Pb/^{206}Pb-corrected ^{206}Pb/^{238}U ages of 1862 ± 16 Ma (95% confidence). These U–Pb ages are all within error of each other and with Re–Os age data for molybdenite (1853 ± 6 and 1862 ± 6 Ma; Smith *et al.*, 2007), and are therefore considered to be reliable. The titanites define a spread along the concordia from *c.* 1850 to 1750 Ma (Fig. 7c), with a bimodal cumulative probability distribution (Fig. 7e). This may be due to the smaller size of the titanite grains relative to allanite, resulting in enhanced Pb loss, or resetting via dissolution–reprecipitation during subsequent fluid flow events. Both the allanite U–Pb and molybdenite Re–Os ages indicate that sulphide mineralization at Rakkurijärvi occurred at *c.* 1·86 Ga (Smith *et al.*, 2007). The earliest mode in the cumulative probability plot (Fig. 7e) is at ~1880–1860 Ma and

Table 6: Comparison of in-run LA-ICP-MS analyses of basalt glass BCR2G with analysis of USGS BCR2 powder and the published range from microchemical studies (Jochum et al.*, 2005)*

	This study ($n = 14$)		USGS BCR2	Published range	
	Mean	1σ		Min.	Max.
V	443·9	26·4	416·0	380·0	457·0
Mn	2686·5	384·4	1520·0	1780·0	2100·0
Co	36·2	2·4	37·0	35·5	48·8
Ni	14·2	2·0		10·1	51·0
Cu	16·4	1·3	19·0	15·5	66·0
Rb	45·0	3·2	48·0	43·4	63·9
Sr	487·0	158·4	346·0	302·0	357·0
Y	32·7	2·7	37·0	29·0	39·4
Zr	168·1	14·2	188·0	156·0	206·0
Nb	11·1	0·6		10·2	30·4
Mo	155·9	10·7	248·0	231·0	300·0
Ba	553·0	34·0	683·0	571·0	780·0
La	24·9	1·8	25·0	22·4	27·0
Ce	41·6	2·4	53·0	46·0	57·0
Pr	6·1	0·4	6·8	6·1	7·6
Nd	27·8	1·7	28·0	24·5	32·0
Sm	6·4	0·5	6·7	5·9	7·4
Eu	1·9	0·1	2·0	1·6	2·7
Gd	6·5	0·6	6·8	5·5	8·1
Tb	1·0	0·1	1·1	0·9	1·2
Dy	6·5	0·7		5·3	6·8
Ho	1·3	0·2	1·3	1·1	1·4
Er	3·6	0·4		3·1	3·9
Tm	0·5	0·1	0·5	0·4	0·6
Yb	3·6	0·4	3·5	2·6	3·6
Lu	0·5	0·0	0·5	0·4	0·6
Hf	4·8	0·5	4·8	4·4	5·3
Ta	0·8	0·1		0·6	0·9
Pb	11·8	0·9	11·0	9·6	14·8
Th	6·2	0·5	6·2	4·3	6·5
U	1·1	0·1	1·7	1·3	2·1

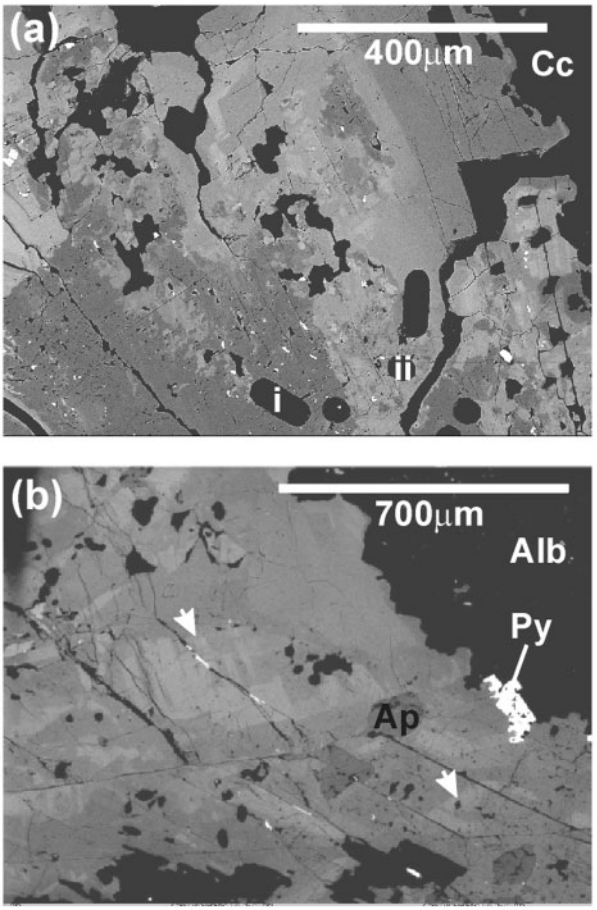

Fig. 4. BSE images of titanite showing key textures indicative of dissolution–reprecipitation and overgrowth. (a) Core–rim boundary of titanite grain from Luossavaara showing dark core with microporous rim, infilled and overgrown by more Fe-rich titanite. i, Laser ablation pit from rastered U–Pb isotope analysis; ii, laser ablation pit from single point trace element analysis. (b) Euhedral titanite from Kallosalmi with relicts of an Fe-rich core replaced by more Fe-poor titanite along fractures and around microporosity (arrows). Alb, albite; Ap, apatite; Cc, calcite; Py, pyrite.

probably records the same event. The later mode is at ~1780 Ma and records Pb loss probably as a result of a thermal metamorphic event.

Samples from the Kallosalmi prospect are hosted by an intensely scapolite–actinolite altered metabasalt (Table 1). Coarse grains of titanite up to 2 mm in diameter occur within the groundmass. The titanite grains are complexly zoned, comprising both BSE dark and light areas that probably represent relict cores surrounded by complex patchy zones and fracture fills that are generally dark or intermediate with some lighter patches. The texture is indicative of dissolution–reprecipitation (Figs 4b and 8a). In all cases common Pb was not detectable (Table 3) and the analyses nearly all overlap concordia (Fig. 8b). There is a spread of $^{206}Pb/^{238}U$ ages along the concordia from *c.* 1950 to 1720 Ma (Table 3; Fig. 8b). Two of the oldest analyses are moderately normally discordant and so, assuming recent Pb loss because of the lack of detectable common Pb, the $^{207}Pb/^{206}Pb$ ages will be slightly older. Plotting all $^{206}Pb/^{238}U$ ages on a cumulative probability density plot (Fig. 8c) shows the data to be bi- or multi-modal, with the oldest mode at *c.* 1950 Ma. $^{207}Pb/^{235}U$ and $^{207}Pb/^{206}Pb$ ages for the oldest analyses are older than the $^{206}Pb/^{238}U$ ages (i.e. discordant), and may indicate that some parts of the grain preserve ages older than 2000 Ma, representing

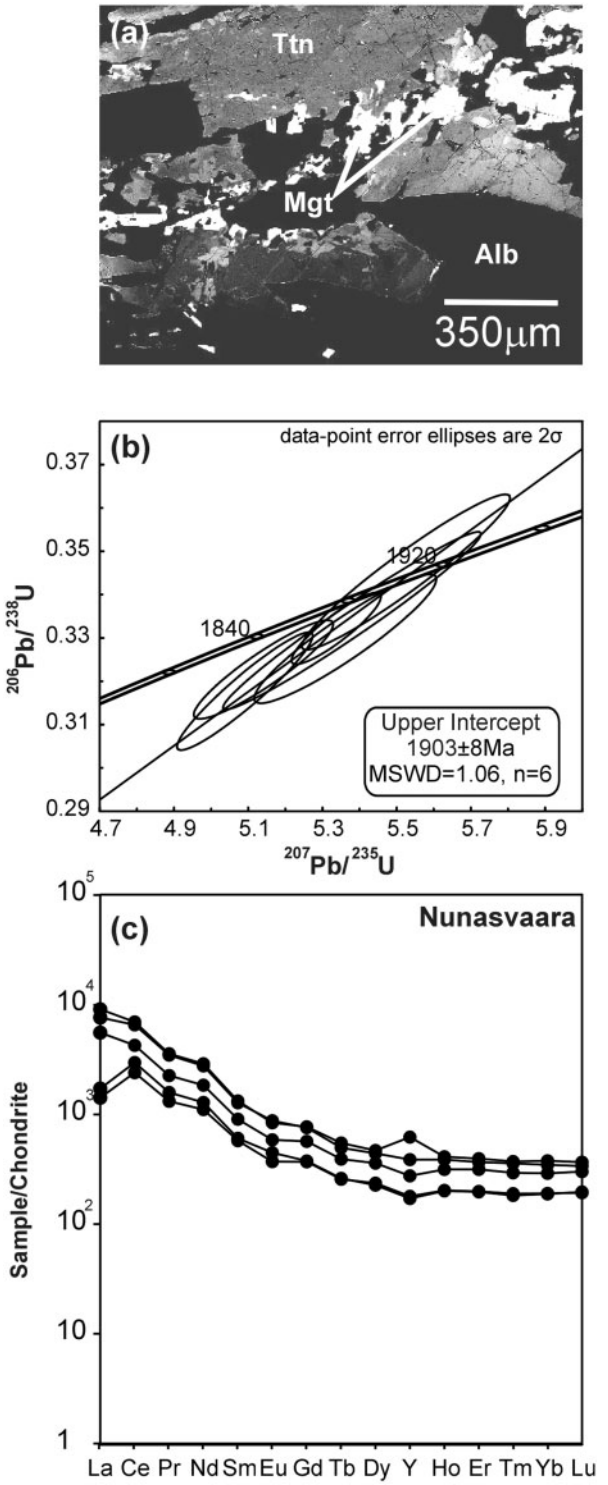

Fig. 5. (a) BSE image of representative titanite from Nunasvaara (03NUN30). (b) U–Pb concordia diagram for analyses of Nunasvaara titanite. (c) Chondrite-normalized REE patterns for Nunasvaara titanite [chondrite values from Wakita *et al.* (1971) here and throughout].

core relicts of earlier thermal events affecting the Greenstone Group (see Storey *et al.*, 2007). The younger modes occur around ages of *c.* 1850 Ma and 1760 Ma (Fig. 7); a weighted average of the $^{206}Pb/^{238}U$ ages (Fig. 8b) gives an age of 1791 ±24 Ma.

Samples from the Nautanen prospect come from the main NDZ. In sample NAU84012 159.8m titanite grains, ranging from 1 to 2 mm in diameter (Fig. 9a), occur in a well-foliated epidote–actinolite–albite schist, and are aligned with the schistosity. They are typically compositionally homogeneous, with some fracturing. Allanite is euhedral to subhedral, occasionally rimmed by epidote, and shows internal zonation, with some evidence of core corrosion prior to overgrowth by epidote (Fig. 9b). U–Pb titanite and allanite analyses cluster about the concordia (Fig. 9c) and define a single mode (Fig. 9d and e), yielding a weighted average of $^{206}Pb/^{238}U$ ages of 1777 ±20 Ma. One allanite analysis is much younger at *c.* 1580 Ma (Table 3). In sample NAU77006 164.28m titanite is associated with scapolite–actinolite–albite alteration, overprinted by epidotization. Titanite in this sample is zoned, with small patches of BSE light titanite (possibly relicts of an original core) surrounded by BSE darker titanite, which notably occurs around fractures and areas of internal porosity (Fig. 10a). U–Pb analyses are mostly concordant and unimodal (Fig. 10b and c), and yield a combined weighted average $^{206}Pb/^{238}U$ age of 1785 ±21 Ma. These two independent ages from Nautanen are identical and suggest an event at *c.* 1780 Ma. The range of ages indicated at Nautanen is comparable with the *c.* 1800–1780 Ma deformed alteration and vein-assemblages identified as a part of a recent study of the Aitik deposit by Wanhainen *et al.* (2005), which indicated several thermal and hydrothermal events affecting the deposit from 1888 to 1728 Ma.

Major element chemistry of titanite and allanite

The major element compositions of titanite by electron microprobe are summarized in Table 4, and plotted in Fig. 11. The primary variations in chemistry responsible for the zonation in titanite are the contents of Fe (calculated as Fe^{3+}) and Al^{3+} (Fig. 11a and b). F contents were not routinely determined as a part of the analyses, but rarely exceed 0·37 wt % (~0·15 a.p.f.u., Table 4). The REE show a negative correlation with Ca (Fig. 11c), with a ratio of ~2Ca:1REE, suggesting the substitution of the REE onto the Ca site (Ribbe, 1980). Positive correlations with Na and Fe (Fig. 11d and e) suggest substitution mechanisms such as $[Ca^{2+}]_{-2}[REE^{3+}]_{+1}[Na^{+}]_{+1}$ and $[Ca^{2+}]_{-1}[Ti^{4+}]_{-1}[REE^{3+}]_{+1}[M^{3+}]_{+1}$ (Ribbe, 1980). Allanite was analysed from Rakkurijärvi and Nautanen (Table 5, Fig. 12). Rakkurijärvi allanite is dominated by the ferriallanite component, whereas at Nautanen compositions are closer to an REE-bearing epidote with a slight excess of Al relative to Fe^{3+} (Fig. 12; Petrik *et al.*, 1995).

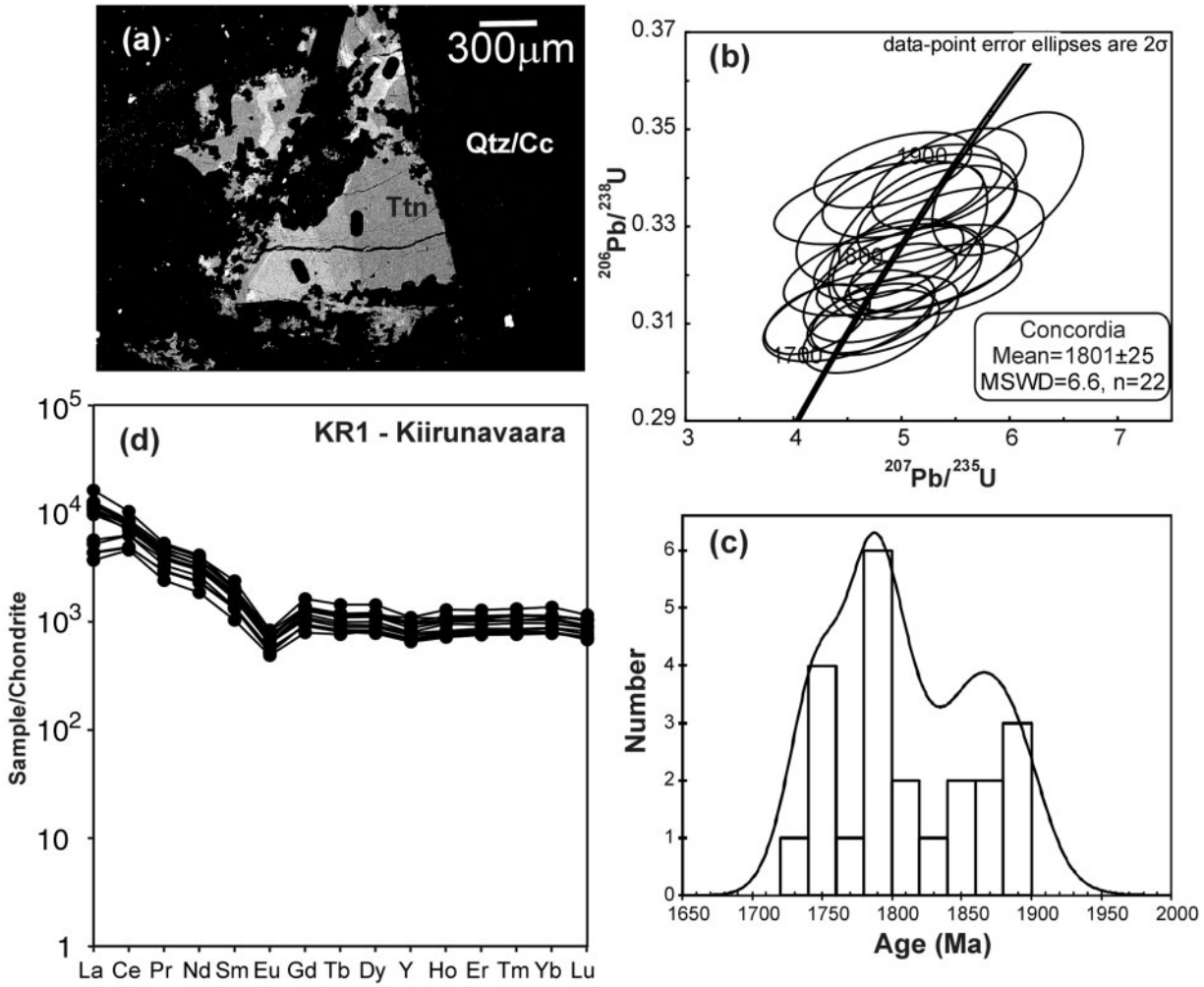

Fig. 6. (a) BSE image of representative titanite from Kiirunavaara (KR1). (b) U–Pb concordia diagram for analyses of Kiirunavaara titanite. (c) Cumulative probability diagram for Kiirunavaara titanite. (d) Chondrite-normalized REE patterns for Kiirunavaara titanite.

Trace element chemistry of titanite and allanite

The results of trace element analyses are summarized in Table 7, and illustrated in Figs 5–10 and 12–16. Y is plotted as a pseudolanthanide (Bau, 1996). Trace element data for the two samples that did not yield reliable U–Pb ages are shown in Fig. 13. Variations in the REE patterns of titanite are indicated in Fig. 16 using plots of Eu anomaly $\{Eu/[0{\cdot}5(Sm+Gd)]\}$ and Y anomaly $[Y/0{\cdot}5(Dy+Ho)]$ vs Ce/Lu. The Ce/Lu ratio was used to indicate the general level of relative LREE enrichment as La shows variable depletions in different samples. The full dataset is available in Electronic Appendix 2.

Fe oxide–apatite deposits

At Luossavaara and Gruvberget titanite is strongly zoned; the core to rim contrast in trace element chemistry is most marked for the REE, with the rims being markedly enriched in the LREE relative to the cores (Fig. 14; Storey *et al.*, 2007). The rims are also enriched in other HFSE (Zr, Hf, Nb, Th); Th is enriched relative to U, and V is enriched relative to other the deposit types (Fig. 15). The trace element patterns from the sample from Kiirunavaara are similar to those of the rims of the Luossavaara sample, but with higher contents of Zr and Hf. The sample from Malmberget is distinct from the Kiruna area samples in terms of its REE pattern, and in having relatively higher contents of Ta and U. Most titanites from Fe-oxide–apatite deposits (excepting distinct grain cores) show negative Eu anomalies and positive Y anomalies with a trend of increasingly negative Eu with decreasing Ce/Lu ratio (Fig. 16). The sample from a late-stage quartz vein at Kiirunavaara is distinct in terms of its slightly negative Y anomaly. La is depleted relative to Ce at Gruvberget and Malmberget.

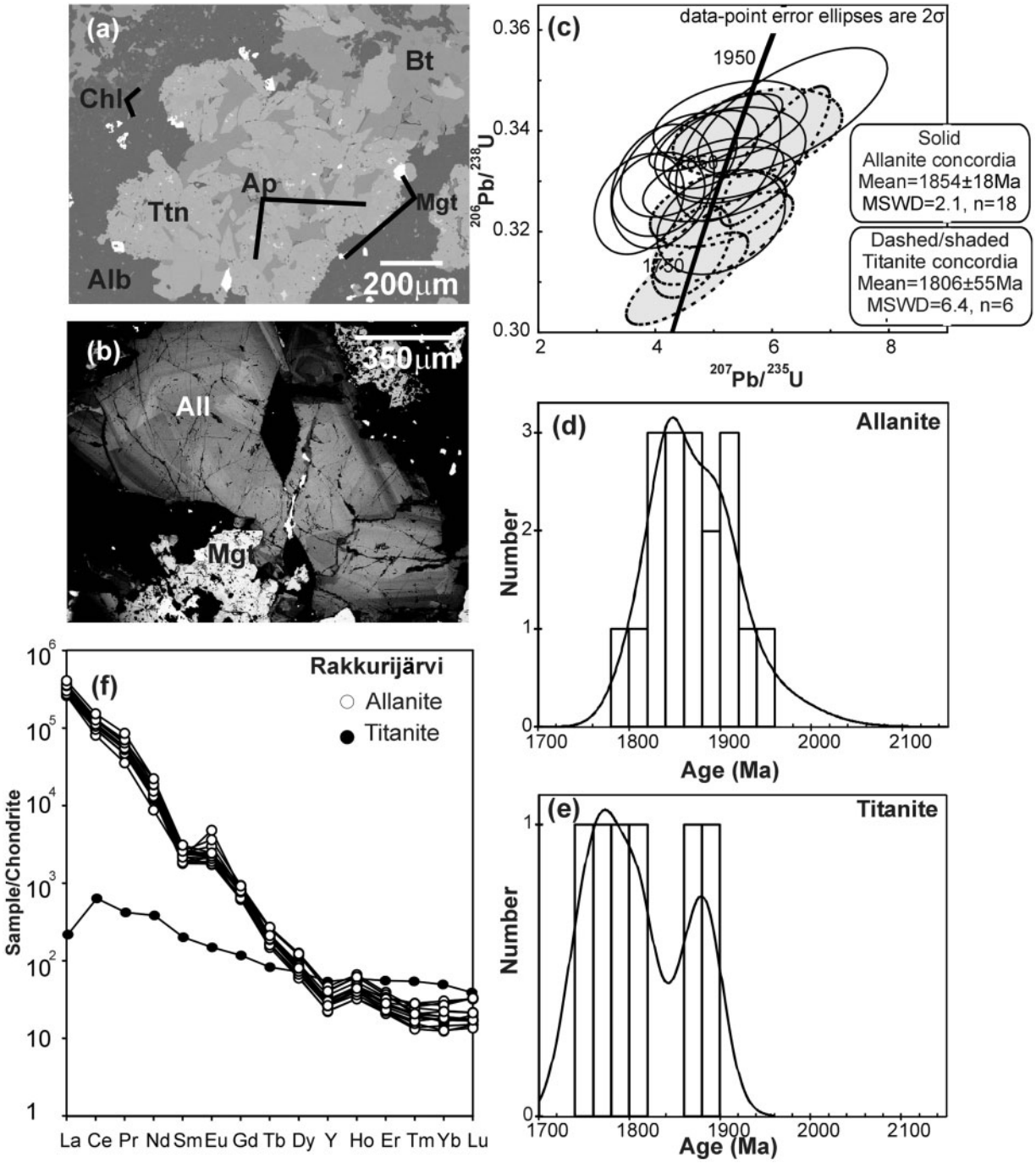

Fig. 7. (a) BSE image of titanite from Rakkurijärvi sample 01RAK006 183.2m. (b) BSE image of allanite from Rakkurijärvi sample 01RAK006 183.2m. (c) U–Pb concordia diagram for analyses of Rakkurijärvi allanite and titanite. (d) Cumulative probability diagram for Rakkurijärvi allanite. (e) Cumulative probability diagram for Rakkurijärvi titanite. (f) Chondrite-normalized REE patterns for Rakkurijärvi allanite and titanite.

Porphyrite, Kiirunavaara and Greenstone Group hosted IOCGs

In the samples from the relatively undeformed Cu–(Au) deposits hosted by the Porphyrite, Kiirunavaara Porphyries and Greenstone Groups, similar REE and other trace element patterns are seen to those in titanites from the Fe-oxide–apatite deposits, but with some variation. Notably at Sarkivaara, a molybdenite-bearing

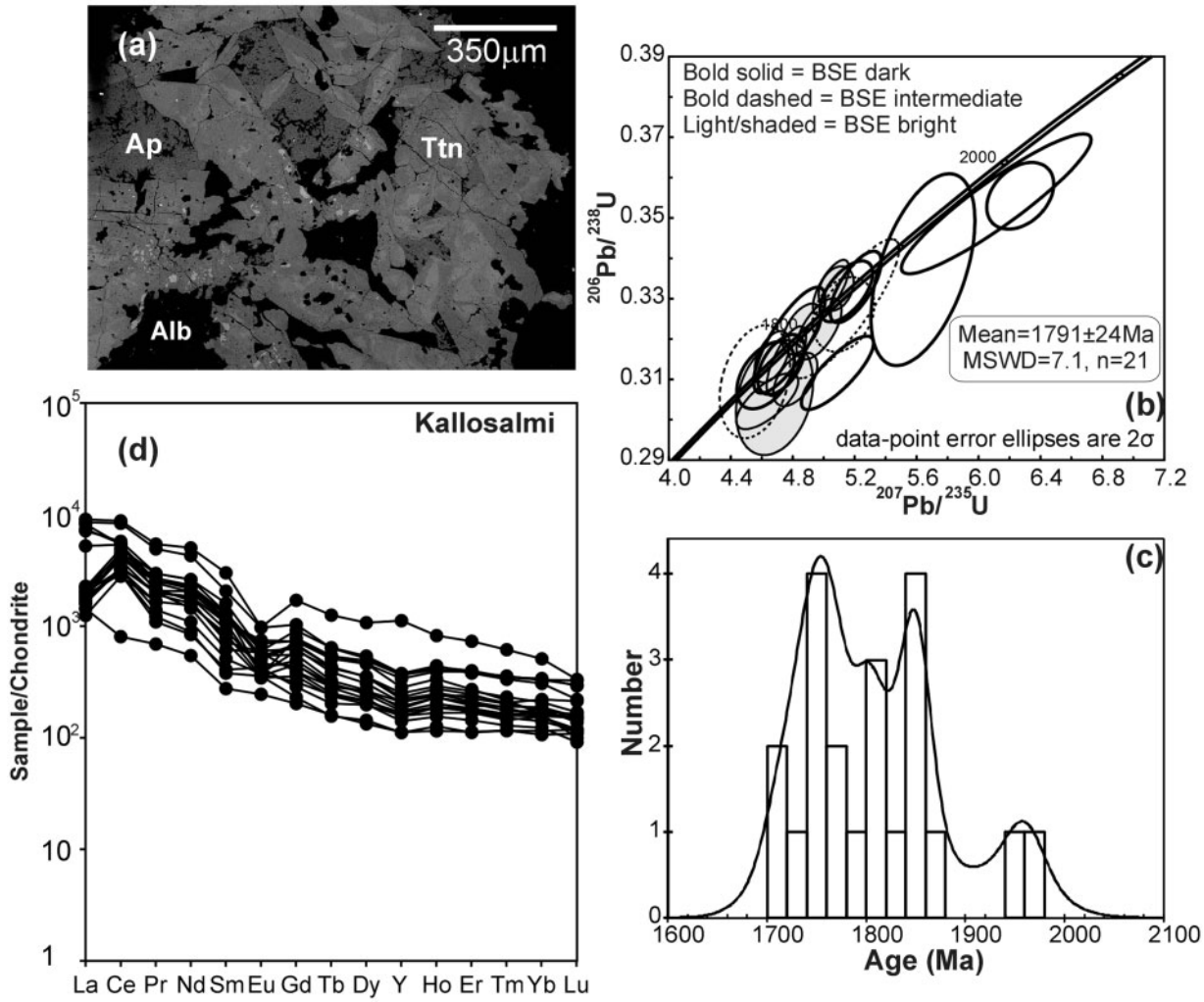

Fig. 8. (a) BSE image of representative titanite from Kallosalmi (KAL90107 56.4m). (b) U–Pb concordia diagram for analyses of Kallosalmi titanite. (c) Cumulative probability diagram for Kalosalmi titanite. (d) Chondrite-normalized REE patterns for Kallosalmi titanite.

prospect, the Mo contents of titanite are elevated relative to other samples. All samples from Porphyrite, Kiiurnavaara and Greenstone Group hosted IOCG deposits are LREE enriched, with negative to positive Eu anomalies, and negative to no Y anomaly, distinguishing them from the Fe oxide–apatite deposits (Fig. 16). At both Sarkivaara (Fig. 13a and b) and Kallosalmi a trend from La-enrichment to La-depletion relative to Ce occurs, accompanied by an increasingly positive Y anomaly at Sarkivaara, and absent to positive Eu anomaly.

NDZ hosted IOCGs

The deposits associated with the NDZ are markedly different in terms of their titanite REE patterns and show elevated U, Mn and Ni contents. The HFSE show similar enrichment to titanites from other deposits (Fig. 15). At both Nautanen and Aitik titanite is consistently LREE depleted relative to heavy REE (HREE) (Figs 9f, 10d and 13d). Eu anomalies are absent to slightly positive, and whereas Aitik shows no Y anomaly, titanite from Nautanen shows a marked positive anomaly in some cases (Fig. 16). The contrast in REE chemistry is also mirrored in the chemistry of allanite from Rakkurijärvi and Nautanen, which, although consistently LREE-enriched, show different levels of enrichment relative to the HREE (Figs 7f and 9f).

DISCUSSION

Origin and paragenesis of titanite and allanite

Fe oxide–apatite deposits

Globally Fe oxide–apatite deposits have been proposed to have origins ranging from crystallization from a volatile-enriched, oxide melt (e.g. Geijer, 1931; Nyström, 1985;

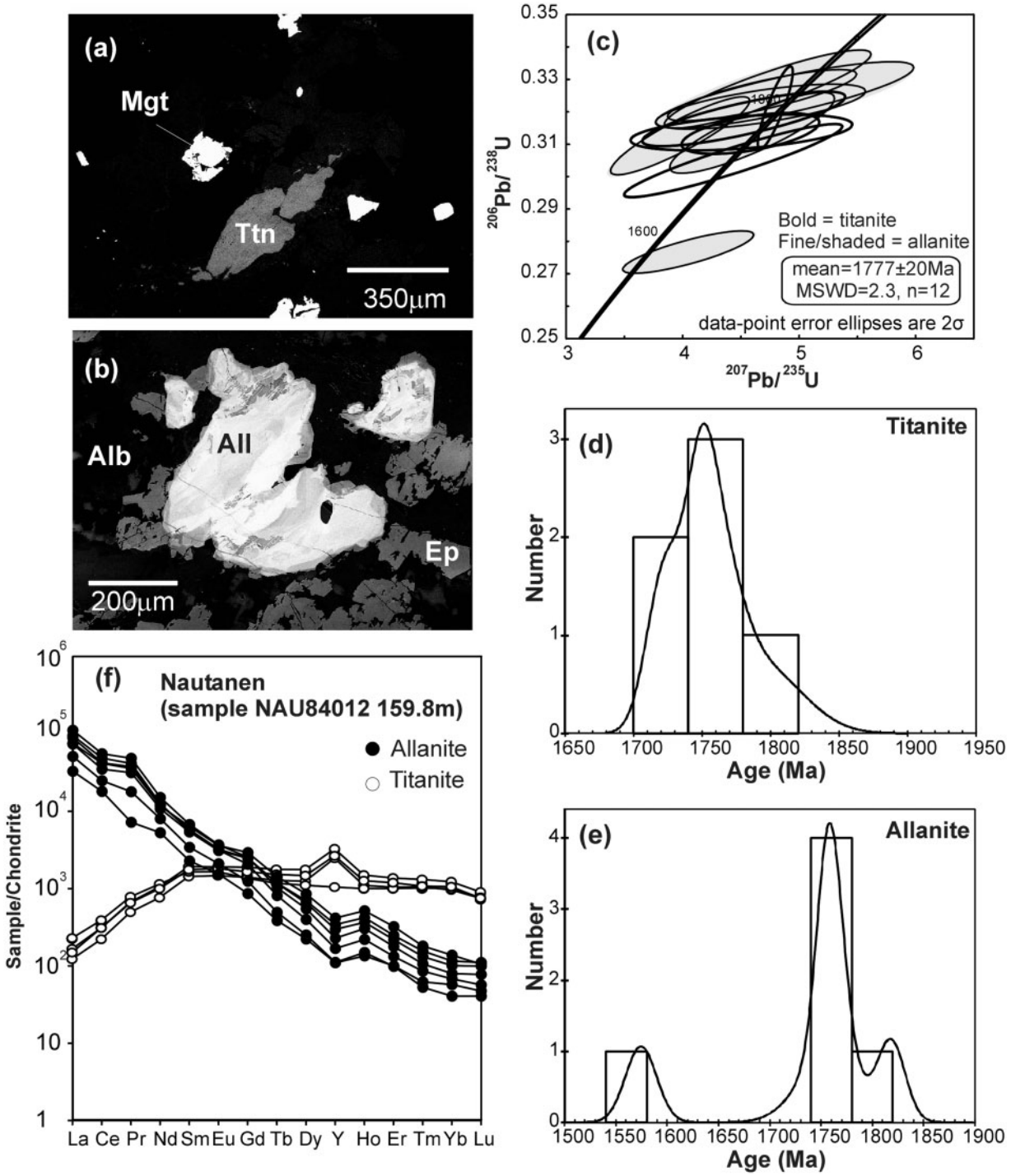

Fig. 9. (a) BSE image of titanite from Nautanen sample NAU84012 159.8m. (b) BSE image of allanite from Nautanen sample NAU84012 159.8m. (c) U–Pb concordia diagram for analyses of Nautanen NAU84012 159.8m allanite and titanite. (d) Cumulative probability diagram for NAU84012 159.8m titanite. (e) Cumulative probability diagram for NAU84012 159.8m allanite. (f) Chondrite-normalized REE patterns for Nautanen NAU84012 159.8m allanite and titanite.

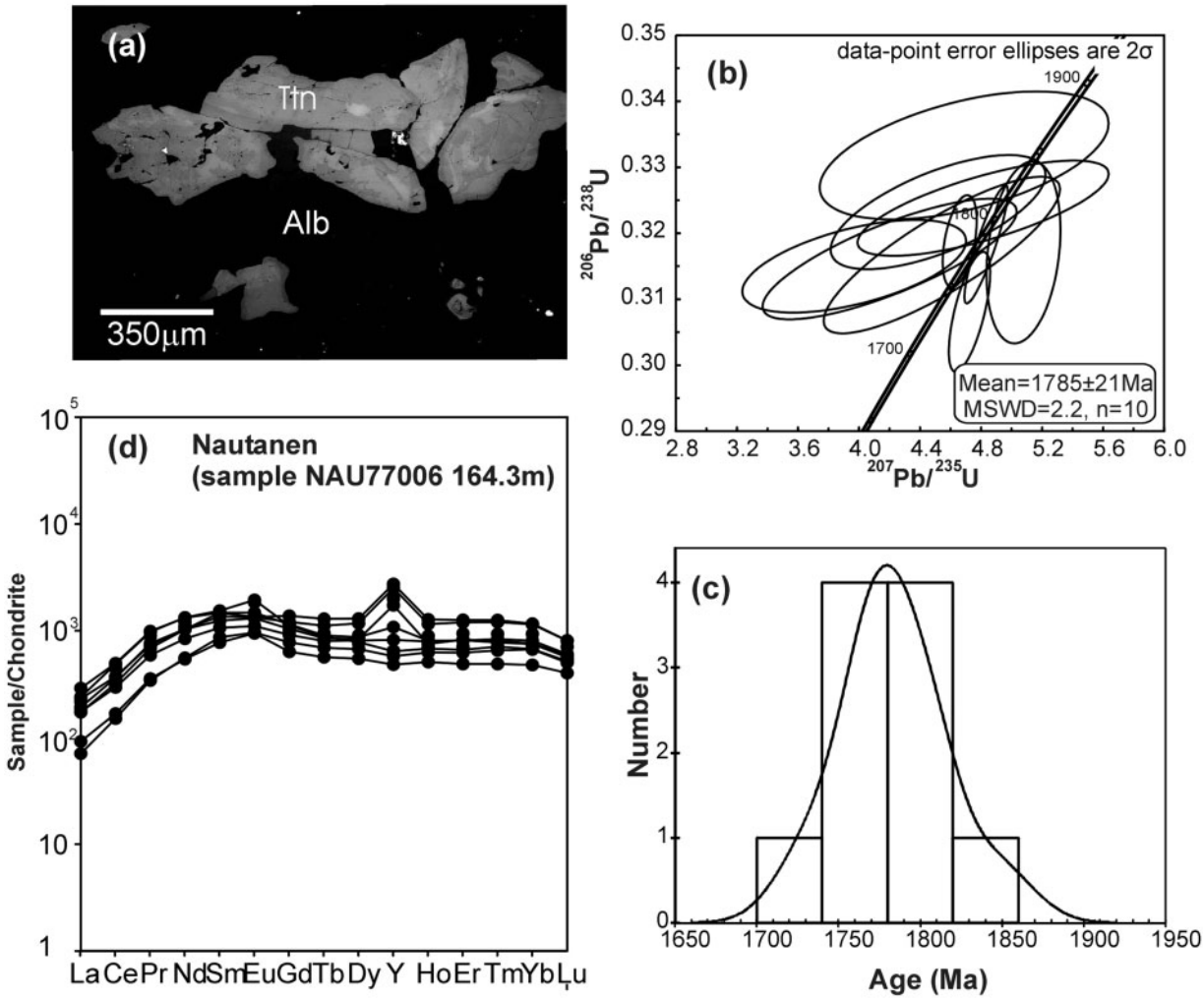

Fig. 10. (a) BSE image of titanite from Nautanen sample NAU77006 164.3m. (b) U–Pb concordia diagram for analyses of Nautanen NAU77006 164.3m titanite. (c) Cumulative probability diagram for NAU77006 164.3m titanite. (d) Chondrite-normalized REE patterns for Nautanen NAU77006 164.3m titanite.

Nyström & Henriquez, 1994; Naslund *et al.*, 2002) to metasomatic replacement or exhalative deposition (e.g. Parak, 1975) involving late-stage magmatic fluids (e.g. Oreskes *et al.*, 1995; Bookstrom, 1995; Sillitoe, 2003) or non-magmatic (evaporite-derived) brines (Barton & Johnson, 1996, 2000). All models unanimously agree on the importance of highly saline hydrothermal fluids, either immediately post-ore formation (Broman *et al.*, 1999; Harlov *et al.*, 2002), or as the main iron-transporting medium (Oreskes *et al.*, 1995; Sillitoe, 2003). The titanite from the Fe oxide–apatite bodies examined in this study formed during two-stage growth (Storey *et al.*, 2007). The cores of grains at Luossavaara and Gruvberget are Fe and trace element depleted, and give much earlier U–Pb ages than grain rims and other ore-related phases (see below), indicating they formed before the main ore depositing stage and thus probably during pre-ore metamorphism (possibly the initial hydrothermal metamorphism) of the volcanic pile. Titanite nucleates on and replaces rutile at Gruvberget (Storey *et al.*, 2007). Early metasomatic assemblages in amygdales involving rutile, quartz and calc-silicate minerals can react to form titanite-bearing assemblages at temperatures between 300 and 500°C, depending on pressure and $X\mathrm{CO}_2$ (Frost *et al.*, 2000). Blake (1990) suggested that the titanite–magnetite–actinolite amygdales at Kiirunavaara and Luossavaara were magmatic exsolution features. The data on timing and textures presented here and by Storey *et al.* (2007) strongly argue against such an origin because of the complex internal zoning and the 100 Myr difference in age between titanite cores and rims. Romer *et al.* (1994) attributed the formation of titanite in amygdales at Kiirunavaara and Luossavaara to post-ore hydrothermal processes, but given the similarities in trace element composition between titanite rims and the apatite

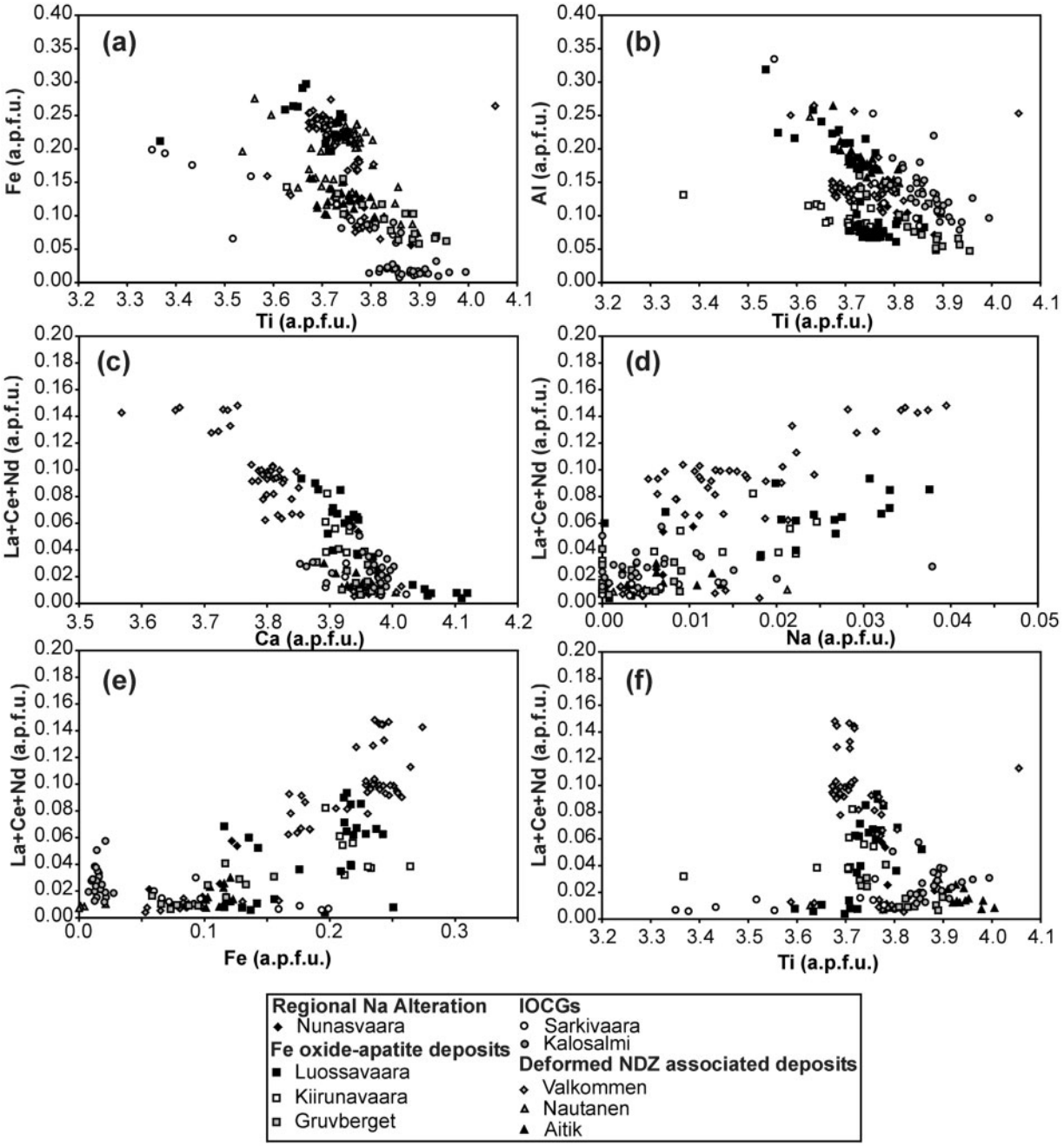

Fig. 11. Variations in titanite crystal chemistry.

in the ore bodies (Frietsch & Perdahl, 1995), these must be closely related to ore formation, either from magmatic fluids exsolved from the crystallizing magnetite ore body or as alteration directly accompanying the hydrothermal formation of the ore. The titanite sampled from Kiirunavaara (KR1) is unequivocally a hydrothermal phase. Titanite at Malmberget undoubtedly formed via similar processes to those operating at Luossavaara and Gruvberget, but the Malmberget deposits are strongly deformed and have been metamorphosed at greenschist- to lower amphibolite-facies conditions (Martinsson & Virkkunen, 2004). The preservation of U–Pb isotopic heterogeneity, rather than complete homogenization during Pb loss, is a result of the relatively high closure temperature (~650–700°C in titanite without radiation damage; Cherniak, 1993; Frost *et al.*, 2000). The trace element

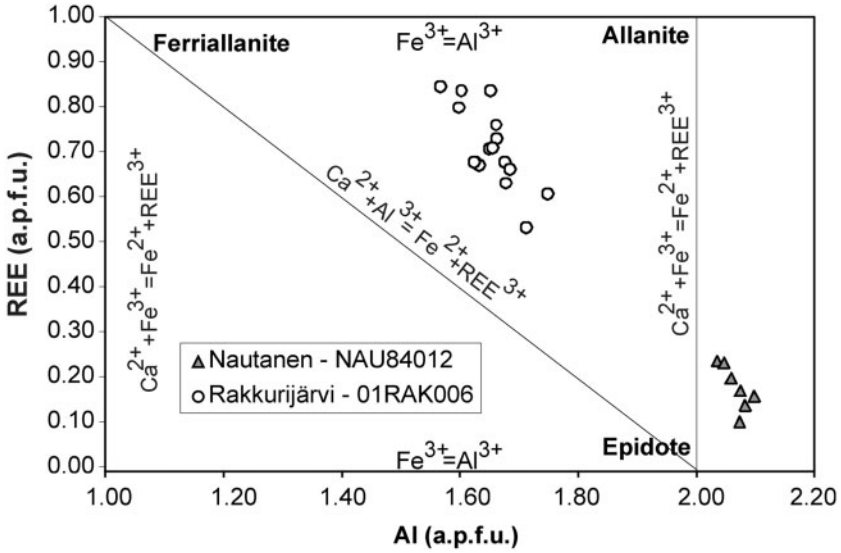

Fig. 12. Variation in total REE vs Al (a.p.f.u.) of allanite. Allanite nomenclature and substitution mechanisms from Petrik *et al.* (1995).

homogeneity of the titanite at Malmberget is almost certainly a primary feature, as the activation energy for REE diffusion in titanite is higher than for Pb (Cherniak, 1995).

IOCGs

The Cu–(Au) deposits studied are all variants of the IOCG type. The only published studies of the formation conditions of IOCG-type deposits in Norrbotten come from Pahtohavare (Lindblom *et al.*, 1996) and the Aitik deposit within the NDZ (Wanhainen *et al.*, 2003), with reconnaissance data being reported by Broman & Martinsson (2000). Preliminary fluid inclusion data from Kallosalmi and Rakkurijärvi indicate similar conditions to those found at Pahtohavare, whereas conditions at Nautanen were at least superficially similar to those at Aitik (Smith & Gleeson, 2005). Minimum P–T conditions for mineralization at Kallosalmi, Rakkurijärvi and Pahtohavare are around 5 kbar and 400°C (Lindblom *et al.*, 1996; Broman & Martinsson, 2000) from fluids with around 45 wt % NaCl eq. All the deposits have undergone metamorphism to some extent (Bergman *et al.*, 2001), although the development of penetrative fabrics is limited to the main deformation zones, and so the fluid inclusions may have been reset. However, stretching of fluid inclusions during deformation typically results in an increase in liquid–vapour homogenization temperature (Vityk, 1995), which would reduce the temperature gap between liquid–vapour homogenization and halite dissolution and hence result in a lower pressure estimate at halite dissolution than in undeformed inclusions (Bodnar, 1994). Equally, fluid loss through leakage would increase estimated salinities. The P estimates on the basis of fluid inclusion data are therefore true minima. At Nautanen early stage fluids were similar to those in the undeformed IOCGs, but fluid circulation along the NDZ continued significantly after the initial mineralization, giving the associated deposits an extended fluid–rock interaction history, involving the superposition of numerous events (Wanhainen *et al.*, 2003, 2005). These constraints are consistent with the hydrothermal formation of titanite syn-ore deposition, but with significant potential for post-formation modification. All deposits show evidence of greenschist-facies metamorphism, but these effects are more pronounced within the NDZ; as noted above, penetrative fabrics are typically limited to deformation zones.

Allanite at Rakkurijärvi and Nautanen is texturally and chemically distinct. At Rakkurijärvi Smith *et al.* (2007) linked allanite formation to high-temperature K–Fe alteration, pre- to syn ore deposition. At Nautanen allanite (strictly an REE-rich epidote) occurs as cores or as zones in epidote grains, and is REE depleted relative to the Rakkurijärvi allanites (Fig. 9). Within the NDZ at Aitik Wanhainen *et al.* (2005) linked epidote alteration to the later stages of the main ore associated alteration.

Timing of magmatism, tectonism and mineralization

Geochronological data from this study are compared with previous results in the context of the timing of the Svecokarelian orogeny in Fig. 17. The implications of concordant U–Pb ages from titanite cores at Luossavaara, Gruvberget and Malmberget have previously been discussed by Storey *et al.* (2007) and indicate a thermal event affecting the volcanic rocks of the Norrbotten district from 2100 to 2000 Ma, suggesting that the volcanic rocks of the Kiirunavaara Group are at least as old as 2100 Ma.

Table 7: Representative results of LA-ICP-MS analyses of trace elements in titanite and allanite

	Nunasvaara	Sarkivaara	Gruvberget		Rakkurijärvi		Kallosalmi	Luossavaara		Nautanen			Kiirunavaara	Vlakommen	Aitik
	03NUN30	SAR1	03GRUV22		01RAK006		KAL90107	03LUOSS01		NAU77006	NAU84012		KR2	03VALK01	A3
			Core	Rim	Titanite	Allanite		Core	Rim		Titanite	Allanite			
V	613·6	1107·0	530·1	1853·1	156·4	598·7	951·7	1309·4	421·2	555·7	600·7	155·0	296·7	292·8	878·6
Mn	122·6	401·3	903·8	345·3	78·9	471·8	96·0	119·3	237·4	1394·6	1136·2	4105·1	266·0	199·5	722·8
Ni	24·6	11·0	9·6	14·7	2·1	11·4	10·9	9·5	10·3	28·6	22·9	17·9	28·8	39·1	33·0
Cu	146·4	6·8	7·7	9·4	2·0	0·7	4·3	20·9	152·8	7·2	12·1	<1·362	14·8	12·8	8·2
Rb	0·7	2·0	0·3	0·7	0·3	0·2	0·4	1·8	2·1	0·7	0·7	0·5	1·0	1·6	0·9
Sr	9·6	13·5	16·7	7·5	3·7	72·7	6·7	4·3	10·7	12·3	7·8	257·8	13·4	12·2	10·5
Y	619·3	152·0	70·9	2475·3	82·6	34·9	570·1	213·1	5065·3	890·4	3249·0	456·8	1239·0	9935·4	1969·6
Zr	312·4	177·1	7·8	123·8	203·7	0·8	51·7	108·5	374·3	63·1	124·0	5·3	2075·5	150·9	206·2
Nb	266·4	57·5	9·1	150·8	164·0	<0·027	141·8	141·1	1586·1	576·2	818·6	<0·052	424·1	1444·8	302·7
Mo	2·3	3·1	3·9	41·7	1·3	<0·174	0·2	2·5	2·7	35·9	52·3	0·3	0·8	5·0	34·7
Ba	3·2	6·2	<0·320	0·3	1·1	1·6	8·6	20·7	4·1	<0·349	<0·338	1·7	4·0	12·0	0·4
La	1843·9	293·9	60·6	305·8	50·0	72784·4	1227·5	41·9	2960·5	16·5	29·8	20680·9	1333·4	1361·5	120·6
Ce	4065·9	931·9	140·0	2080·5	374·1	68676·3	3249·5	127·1	8561·8	90·1	155·6	25223·4	3769·5	6995·0	474·8
Pr	318·2	49·5	21·3	228·8	36·5	5119·7	228·8	32·2	1175·8	30·2	47·6	3330·1	332·5	806·6	144·1
Nd	1285·6	157·0	93·8	1320·3	169·1	7195·9	977·3	193·2	3153·4	249·1	363·3	5416·9	1352·5	4049·6	1038·6
Sm	192·5	21·9	17·3	310·4	28·8	326·9	168·7	60·9	584·5	126·2	205·1	842·4	244·7	1014·7	456·4
Eu	50·4	12·9	3·5	47·6	8·2	97·5	39·2	18·3	143·5	53·1	80·5	177·8	34·6	122·9	160·6
Gd	153·1	23·3	14·9	294·1	22·5	138·3	144·8	57·2	509·3	151·1	257·7	482·6	228·9	1000·6	487·6
Tb	18·5	3·7	1·9	42·4	2·9	6·2	19·5	8·0	76·6	24·8	44·2	41·6	35·9	167·4	71·1
Dy	109·9	24·3	12·1	258·1	17·1	15·1	119·6	47·7	484·5	161·5	284·3	155·5	241·6	1098·2	403·8
Ho	22·1	5·7	2·6	50·8	3·2	1·8	22·8	9·1	97·4	34·5	56·2	20·0	52·7	224·3	75·1
Er	60·0	18·3	7·8	139·2	8·6	3·6	60·9	24·3	279·7	97·7	151·9	34·1	148·2	640·6	199·0
Tm	8·9	3·0	1·2	20·0	1·3	0·3	8·6	3·7	41·7	15·6	20·9	3·1	23·4	97·9	27·1
Yb	58·0	22·6	9·5	129·4	7·9	2·4	53·5	24·3	259·0	107·5	138·1	16·1	156·6	680·1	165·9
Lu	8·4	3·6	1·3	18·5	0·9	0·4	7·2	3·6	36·6	12·1	14·8	2·4	21·1	73·3	18·0
Hf	7·3	10·1	0·3	6·1	7·6	<0·138	5·7	3·1	17·9	4·7	8·1	0·4	138·5	12·8	13·5
Ta	9·3	3·8	0·2	4·7	14·5	0·0	10·4	4·6	24·1	18·7	68·5	<0·054	42·6	600·4	20·5
Pb	39·6	18·9	1·6	9·9	1·9	5·1	9·6	2·5	37·5	1·5	0·6	72·7	35·8	18·2	2·9
Th	201·6	97·1	7·6	71·6	8·0	22·2	54·5	1·9	212·9	7·8	2·0	396·2	201·5	115·7	15·8
U	41·7	81·3	17·9	65·6	2·7	7·2	23·3	29·9	25·6	27·6	104·6	141·6	16·2	79·9	94·0

Previous geochronological constraints suggest these rocks were erupted in the period 1·96–1·88 Ga (Skiöld & Cliff, 1984; Welin, 1987; Cliff *et al.*, 1990; Romer *et al.*, 1994). Storey *et al.* (2007) argued that zircon U–Pb ages in the region of Kiirunavaara may represent resetting, either by volume diffusion because of the small grain size of zircon relative to titanite, or by dissolution–reprecipitation caused by the extreme fluid conditions in the environment of the Kiirunavaara ore bodies. Martinsson (2004) suggested that the chemistry of the Porphyrite Group is consistent with an early Svecokarelian arc environment, whereas the Kiirunavaara Group was interpreted as a bimodal suite linked to within-plate volcanism. We therefore interpret the titanite cores from Luossavaara, Gruvberget and Malmberget to indicate a minimum formation age for the Porphyrite and Kiirunavaara groups pre-2·05 Ga, relating either to early arc formation or to bimodal magmatism (Nironen, 1997; Martinsson, 2004; Wiehed *et al.*, 2005; Fig. 17). The early population at Kallosalmi is also consistent with a thermal event affecting the Greenstone Group at this time. Lahtinen *et al.* (2002) identified a 2·1–2·0 Ga detrital zircon population in sediments from the Central and Southern Svecofennian sedimentary domains in Finland, suggesting the former

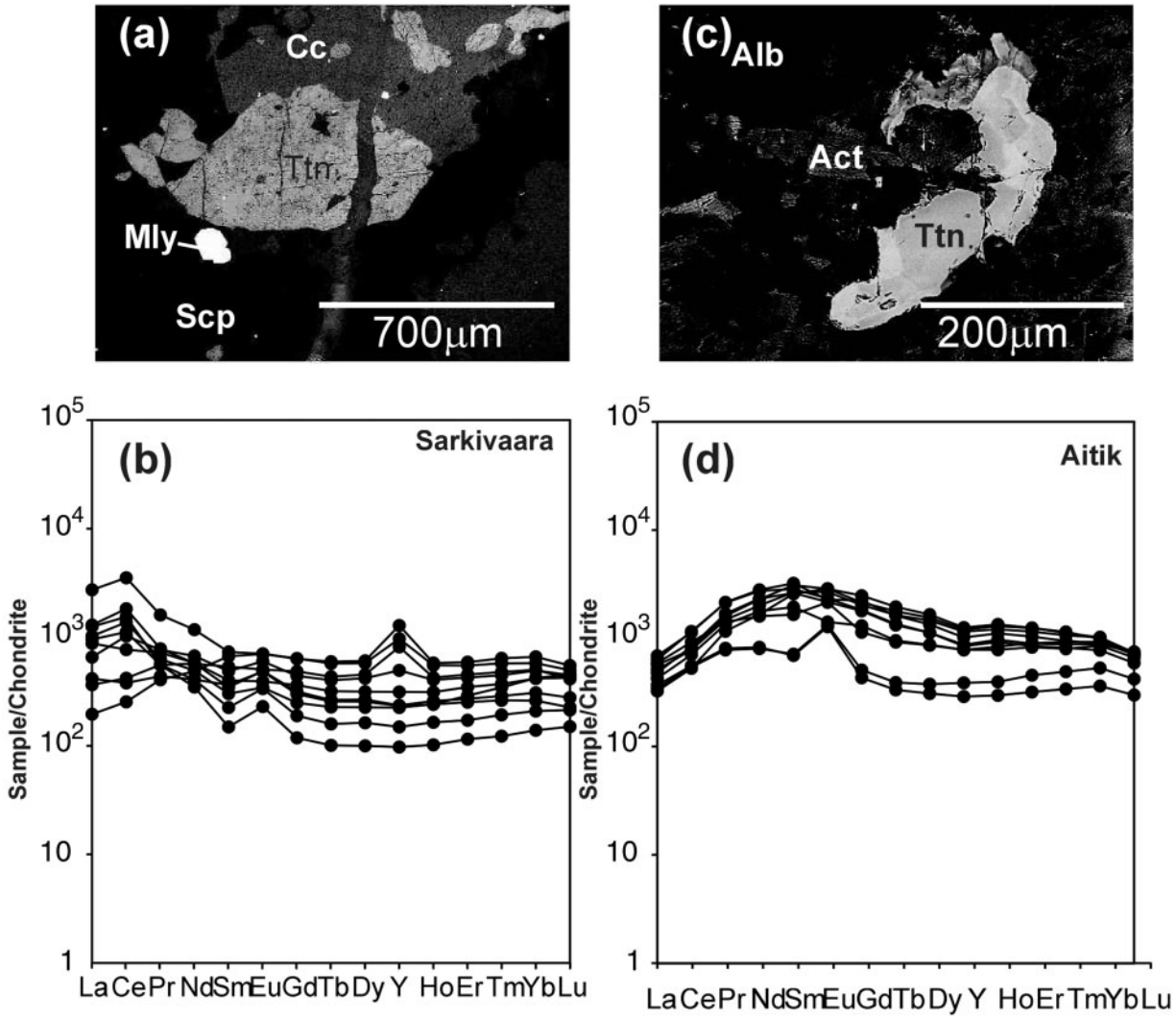

Fig. 13. (a) Representative BSE image of Sarkivaara (SAR1) titanite. (b) Chondrite-normalized trace element patterns of Sarkivaara titanite. (c) Representative BSE image of Aitik (A3) titanite. (d) Chondrite-normalized REE patterns for Aitik titanite.

presence of crust of this age that is now eroded or covered in the Fennoscandian Shield.

This initial stage of mineralization at Malmberget is indicated to have taken place at or before 1920 ± 23 Ma (Storey *et al.*, 2007). This is close in time to, although slightly older than, the timing of Fe oxide–apatite mineralization in the Luossavaara–Kiirunavaara system [1884 ± 6 to 1875 ± 9 Ma, Romer *et al.* (1994); 1870 ± 24 Ma, Storey *et al.* (2007)]. This age range overlaps with the intrusion of the Haparanda and Perthite-monzonite suite granitoids in the Norrbotten region and the initial period of IOCG-type mineralization (Billström & Martinsson, 2000; Bergman *et al.*, 2001). Data from later-stage titanite in the hanging wall breccia at Kiirunavaara also overlap with this time period, but indicate secondary modification of titanite resulting in a spread of ages along concordia as a result of metamorphism or secondary hydrothermal modification. Cliff & Rickard (1992) suggested that sulphide alteration at Kiruna was the result of a late hydrothermal event, dated at ~1·5 Ga using whole-rock Pb–Pb, Rb–Sr and Sm–Nd data. Both Cliff & Rickard (1992) and Romer *et al.* (1994) indicated that the Pb–Pb isotope systematics were probably disturbed, and using a Caledonian event to constrain the lower intercept of a discordia line Romer *et al.* (1994) suggested an alternative interpretation of the same data in terms of metamorphism some time around 1850 ± 80 Ma. Our data strongly support secondary modification of the Kiruna ore system at ~1·8 Ga, corresponding to the period of later Svecofennian granitoid magmatism. Greenschist-facies

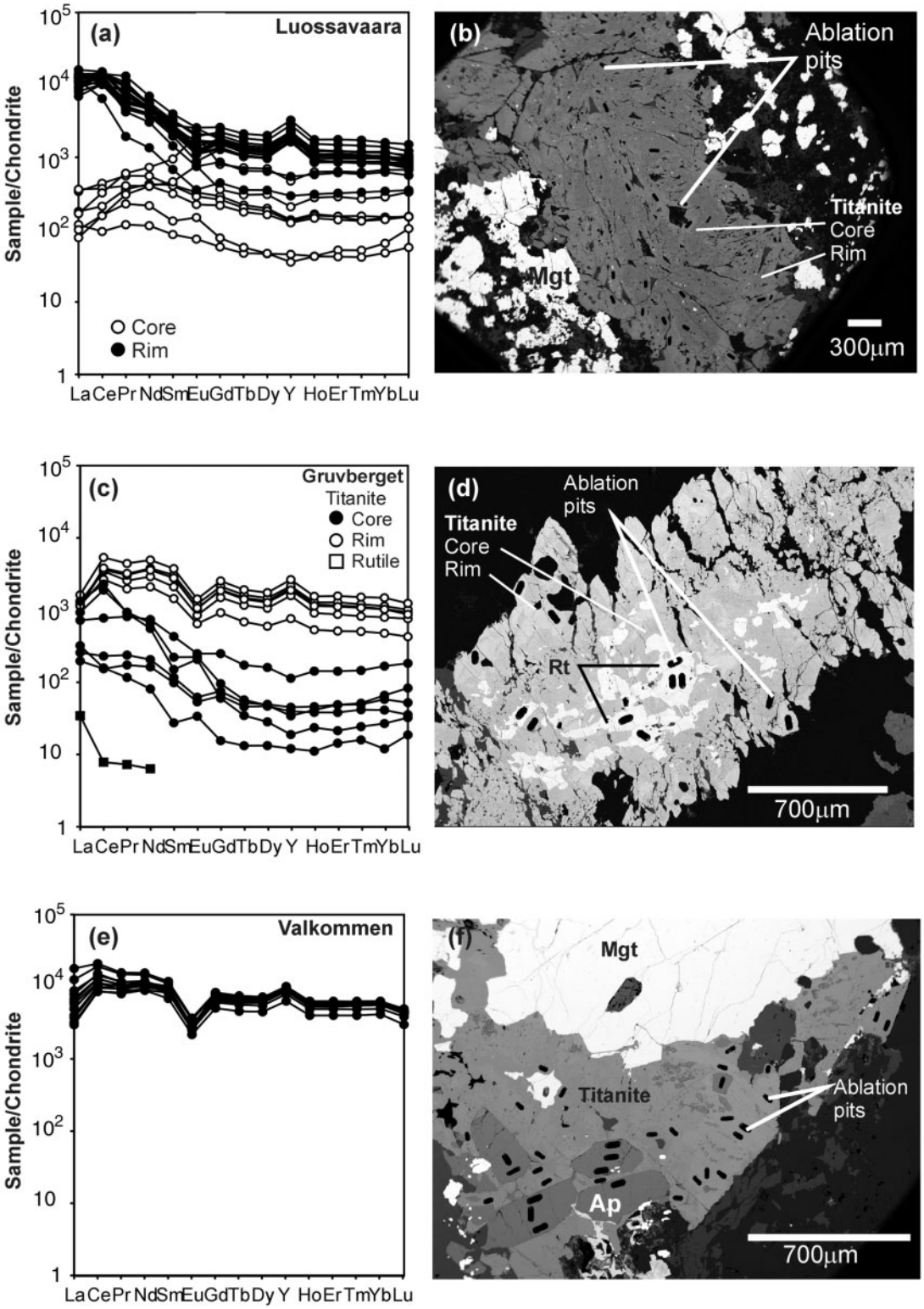

Fig. 14. Chondrite-normalized REE patterns and BSE images of previously analysed titanite. (a, b) Luossavaara. (c, d) Gruvberget. (e, f) Valkommen. Data from Storey *et al.* (2007).

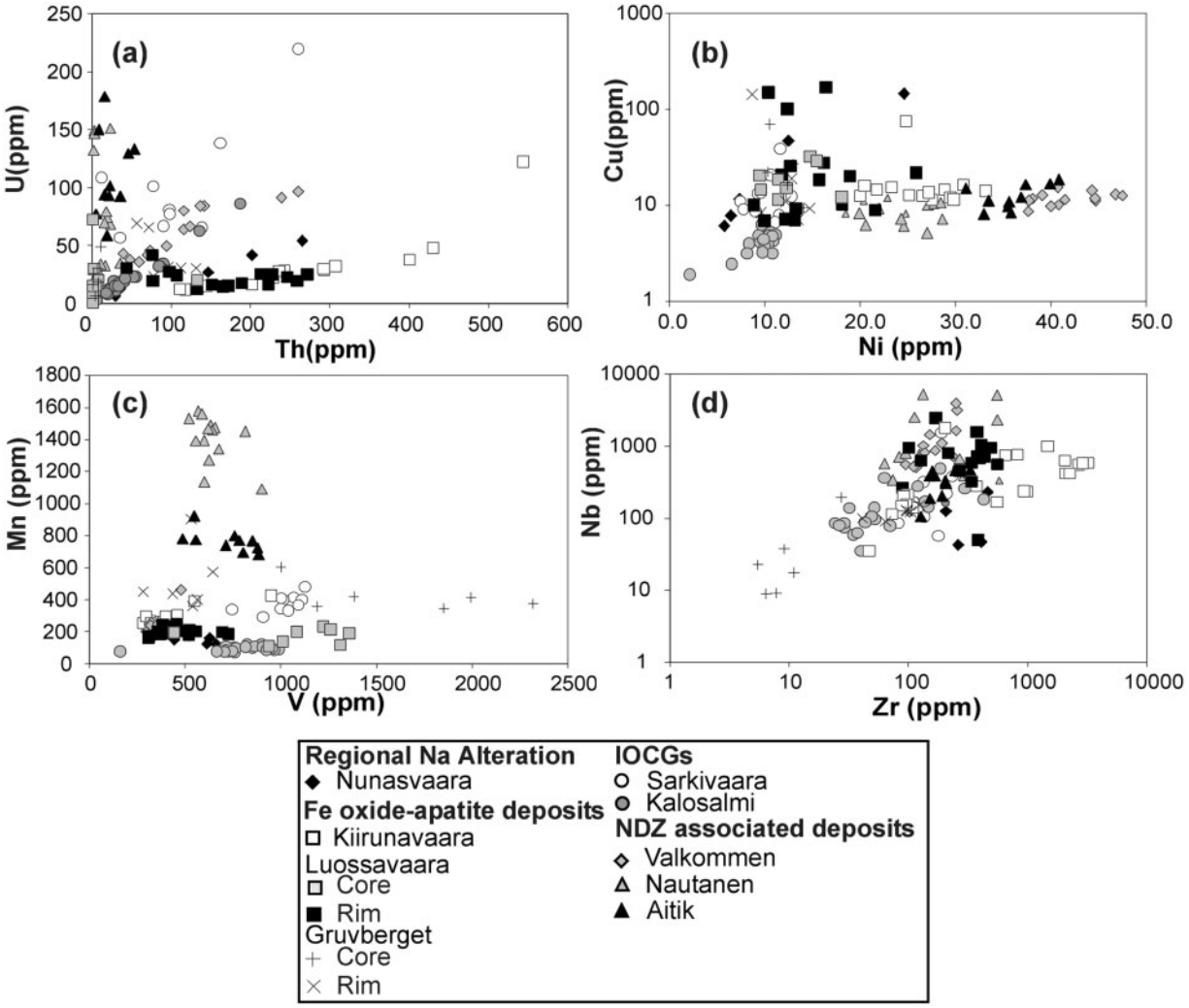

Fig. 15. Variation diagrams for key trace elements in titanite.

metamorphism of the Kiruna area without the development of penetrative deformation has been noted by a number of previous workers (e.g. Nyström & Henríquez, 1994).

Titanite from the regional scapolite–albite alteration exposed at Nunasvaara indicates an age of 1903 ± 8 Ma. This is indistinguishable from the earliest ages at Malmberget and close to the earliest possible ages at Kiirunavaara and Luossavaara. This is significant, as in other IOCG provinces regional scapolite alteration has been proposed to be a distributed metal leaching event which led to the formation of Fe mineralization in structurally focused discharge zones (Barton & Johnson, 1996, 2000; Oliver *et al.*, 2004). A similar model may apply here, but requires more detailed mass-balance studies and a more extensive geochronological study of the regional Na–Ca alteration.

The age of 1854 ± 18 Ma from allanite at Rakkurijärvi overlaps with the age of Fe oxide–apatite mineralization and the early IOCG group identified by Billström & Martinsson (2000), and suggests at least a temporal link between the two. The cumulative probability plots indicate that this represents relatively undisturbed isotope systematics and hence indicates the age of alteration, in good agreement with Re–Os sulphide mineralization ages of 1853 ± 6 Ma and 1862 ± 6 Ma (Smith *et al.*, 2007). The data from titanite are consistent with its metamorphic modification by Pb loss or dissolution–reprecipitation at around 1780 Ma. The data from Kallosalmi are also consistent with metamorphic or metasomatic resetting of titanite formed in the period 1850–1870 Ma at 1750–1780 Ma (Fig. 8). Data from Gruvberget (1820 ± 10 Ma) show little spread along concordia and are interpreted as consistent with mineralization at ~1820 Ma. This is younger than

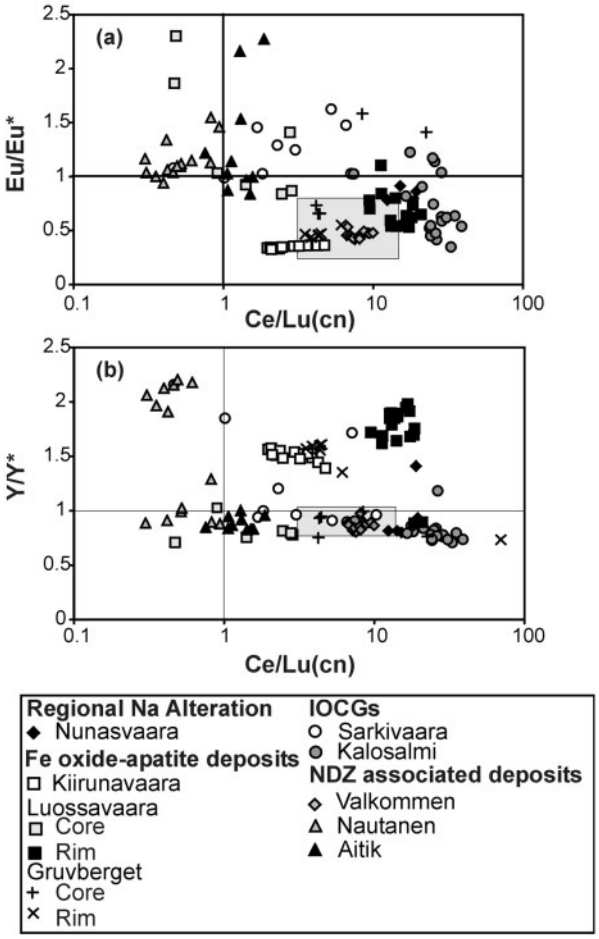

Fig. 16. Variation in Eu and Y anomalies with the slope of the overall REE pattern [Ce/Lu(cn)]. Eu anomaly $Eu/Eu^* = Eu/[0{\cdot}5(Sm + Gd)]$; Y anomaly $Y/Y^* = Y/[0{\cdot}5(Dy + Ho)]$. Shaded boxes indicate the range in compostion of apatite from Frietsch & Perdahl (1995) and Harlov *et al.* (2002). cn, chondrite-normalized.

dates for other deposits from this study and others, and hence indicates more than one episode of mineralization across the area. The early Fe-oxide–apatite mineralization at Gruvberget may be of a similar age, or may be older.

The data from titanite and allanite at Nautanen overlap with the younger (1800–1750 Ma) group of IOCG-type deposits identified by Billström & Martinsson (2000) and are in agreement with the detailed study of the nearby Aitik deposit by Wanhainen *et al.* (2005), which recognized an initial, possibly porphyry-Cu style, mineralization constrained to be within the period 1876 ± 10 Ma to 1848 ± 8 Ma, overprinted by a more complex alteration assemblage at some time around 1780 Ma. The later stage is also recorded at Nautanen and appears to represent a thermal event(s) related to fluid flow along the NDZ and associated structures.

The time constraints currently available bracket different stages of mineralization, but are currently very broad as the complex geological history has resulted in variable resetting of the isotope systematics of a range of phases. More precise analytical techniques (TIMS) do not resolve this issue, as previous studies have averaged some of the intracrystalline variation seen in this study and given by Storey *et al.* (2007). Overall the data presented here are consistent with regional scapolite alteration in the period 1911–1895 Ma, although this is constrained by only a single sample. Iron oxide–apatite mineralization took place at some point in the period 1920–1870 Ma, and was overprinted by later fluid flow events; these were probably responsible for sulphide mineralization, which resulted in some resetting of earlier formed titanite within the period 1870–1830 Ma. There is evidence for mineralizing events down to 1820 ± 10 Ma. Most of the deposits studied preserve evidence of a thermal metamorphic event within the period 1750–1780 Ma. For deposits within the NDZ titanite and allanite grains were either completely reset, or initially crystallized, within this period, probably during movement and fluid flow along the shear zone. This period corresponds to the 1770–1800 Ma late Svecofennian deformation and metamorphism identified by Bergman *et al.* (2001) and current constraints on the intrusion period of the Lina suite granitoids (Skiöld, 1988). In models of the tectonic evolution of the Svecofennian this period also brackets the post-accretion transition from intra-cratonic transpression to orogenic collapse, which may have caused reactivation of existing structures (Nironen, 1997; Weihed *et al.*, 2005; Fig. 17).

Trace element characteristics of titanite and allanite

The trace element patterns of hydrothermal minerals can be affected by the composition of the metal source, equilibrium mineral–fluid partitioning (McIntire, 1963), the ligand chemistry of the hydrothermal fluid (Haas *et al.*, 1995), and the kinetics of mineral growth and dissolution (Möller, 1998). They can also be affected by the redistribution of the REE between phases, with or without bulk addition or leaching of the REE, during metamorphism or metasomatism. In this study, except for variations in trace element patterns between clearly distinct stages of crystal growth, intracrystalline variations in trace element chemistry are minor compared with variations between deposits, suggesting that kinetic factors were of limited importance. Diffusive rehomogenization of titanite trace element patterns on geologically realistic time scales is extremely unlikely at temperatures below 800°C (Cherniak, 1995). The grains studied therefore probably preserve the original variation in trace element chemistry, except in the case of rehomogenization by dissolution–reprecipitation processes. Comparison between the effective ionic radius of Ca^{2+} and the trivalent REE in sevenfold coordination from recent thermodynamic models for

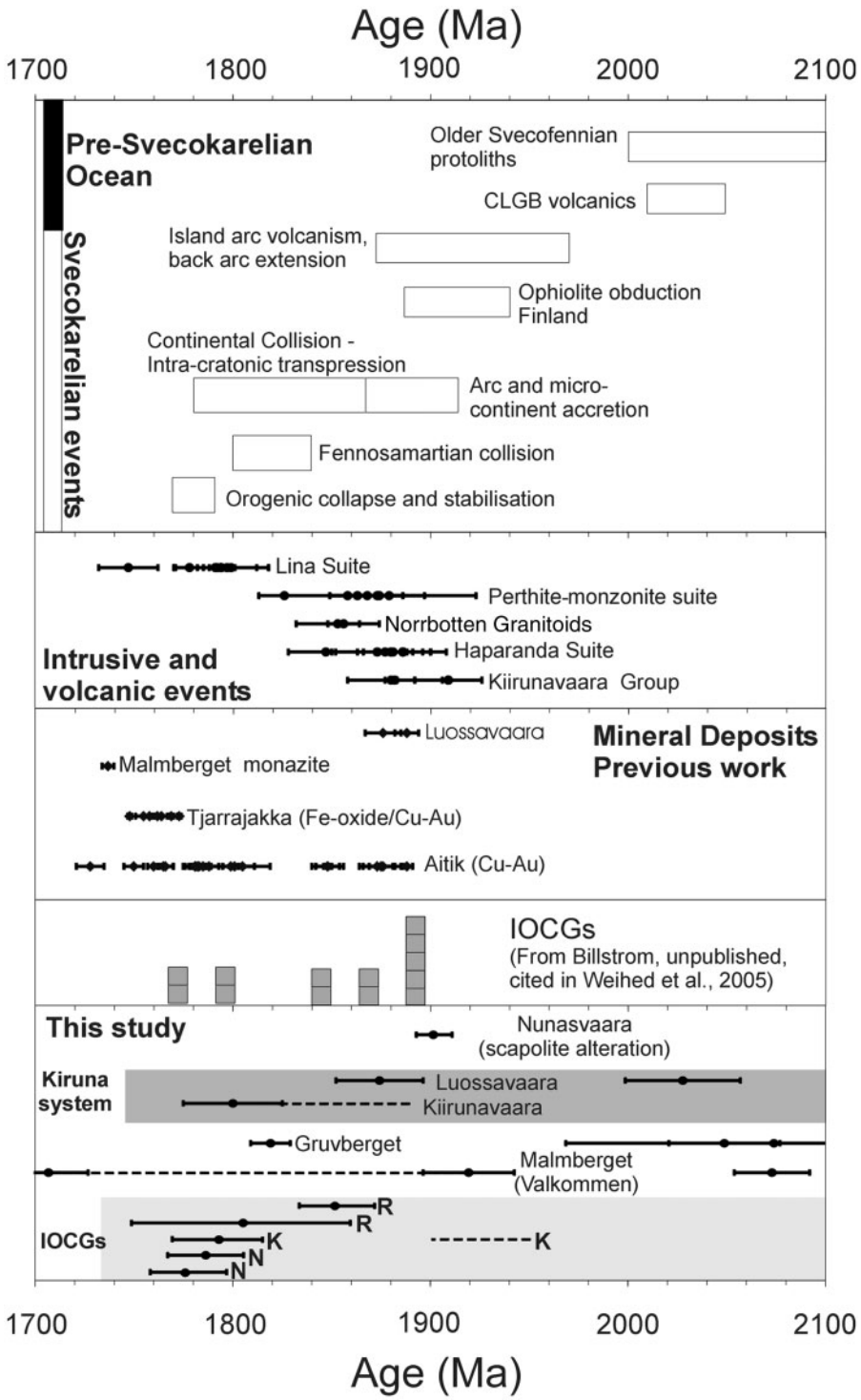

Fig. 17. Summary of key events in the evolution of the Fennoscandian Shield compared with previous geochonological data from the Norrbotten region and this study. Data from the reviews of Nironen (1997), Bergman *et al.* (2001) and Weihed *et al.* (2005). Other data from Romer *et al.* (1994) (Luossavaara); Romer *et al.* (1996) (Valkommen); Lahtinen *et al.* (2002) (older Svecofennian protoliths); Edfelt *et al.* (2005) (Tjårrajåkka); Wanhainen *et al.* (2005) (Aitik). Data for other IOCGs are unpublished data from K. Billström cited by Weihed *et al.* (2005). K, Kallosalmi; R, Rakkurijärvi; N, Nautanen. Points indicate weighted mean ages from this study, except in the case of Malmberget where limiting single analyses are shown. Dashed lines indicate either single analyses or ranges inferred from the spread of data along concordia and cumulative probability plots.

titanite–melt fractionation (Tiepolo *et al.*, 2002; Prowatke & Klemme, 2005) shows the closest correspondence in radii between Ca and Sm, Eu and Gd, whereas estimates from Shannon (1976) show the closest correspondence with Ce. Values are not reported for Pr and Nd. Purely on the basis of spatial accommodation into the titanite lattice this would suggest that, in the absence of fluid speciation control, titanite–aqueous fluid partitioning should lead to preferential incorporation of the middle REE (MREE) into titanite, with relatively low La contents relative to Ce. These considerations account for a number of the features of the REE patterns observed in titanites from this study. Of the other trace elements analysed in this study most bivalent ions will also substitute onto the Ca-site (including Cu, Mn, Sr) as will U and Th. Other tetravalent, or higher oxidation state cations (e.g. Zr, Nb, Ta) will usually substitute for Ti^{4+} (Ribbe, 1980).

The trace element patterns in titanite cores from Luossavaara and Gruvberget are consistent with these partitioning constraints and suggest crystal chemically controlled REE partitioning during metamorphic formation of titanite (Storey *et al.*, 2007). The titanites studied here are strongly LREE enriched relative to these grain cores. Bulk-rock data from unmetasomatized equivalents distal from the ore bodies is lacking in most of the examples studied here, but metasomatic addition of the REE and other trace elements, hosted by apatite, titanite and allanite, has been demonstrated at Tjårrajåkka (Edfelt *et al.*, 2005). This mechanism is favoured here as in at least one example (KR1) titanite is vein hosted, and therefore the trace element content must represent REE transported in a hydrothermal fluid. The REE patterns of titanite are also similar to those reported from apatite from the same or similar deposits (Frietsch & Perdahl, 1995; Harlov *et al.*, 2002; Edfelt *et al.*, 2007; Fig. 16). Studies of coexisting apatite and titanite in the literature suggest that equilibrium partitioning should result in apatite with LREE enrichment relative to titanite (Henderson, 1980), and so the similarity in chemistry suggests external fluid control.

The rims of titanite at Luossavaara (Storey *et al.*, 2007) and grains from Kiirunavaara are LREE enriched, and have low U/Th ratios and high Zr and Nb concentrations. The latter characteristics might argue strongly for the magmatic origin of the titanites in the Kiruna deposit, as these elements are generally considered to be immobile, or at least conserved, in hydrothermal systems. However, both samples are hydrothermal in setting, and both show anomalous behaviour of Y relative to Dy and Ho. This is consistent with the influence of aqueous speciation on REE chemistry, and in particular the formation of M^{3+}–F complexes (Bau, 1996). The high Zr and Nb in titanite from different stages of the Kiruna system indicates that these elements were mobilized in the hydrothermal phase (e.g. Gieré, 1986; Salvi & Williams-Jones, 1990, 1996). The high-temperature conditions and extreme salinities of fluids in all deposits may have promoted HFSE mobilization as aqueous chloride complexes; high F activities may also significantly enhance the solubility of HFSE, including Zr and Nb in hydrothermal solutions (e.g. Gieré, 1990; Rubin *et al.*, 1993; Gagnon *et al.*, 2004; Smith, 2007). Apatites from Fe oxide–apatite deposits are notably enriched in F relative to Cl, whereas those from IOCG-type mineralization are typically Cl-rich (Frietsch & Perdahl, 1995; Edfelt *et al.*, 2005, 2007). This indicates higher HF activities in Fe oxide–apatite deposit related fluids (Korzhinskiy, 1981). High HF activity in Fe oxide–apatite mineralizing fluids may also account for the LREE enrichment of associated titanite, as aqueous LREE–F complexes are more stable at high P–T than those of the HREE (Haas *et al.*, 1995). Titanite from Malmberget is LREE depleted relative to that from Kiirunavaara. This may result from dissolution–reprecipitation of titanite during metamorphism, as the LREE may be preferentially lost to the fluid during such a process. Harlov *et al.* (2002) noted LREE-depleted-zones in apatite from Kiirunavaara surrounding monazite inclusions formed during greenschist-facies metamorphism.

Within the IOCG deposits, those Porphyrite, Kiirunavaara and Greenstone group hosted deposits in the general area of Kiruna are similar in terms of their LREE enrichment, but show distinct negative Y anomalies (Fig. 16b). The titanite from regional Na–Cl altered rocks at Nunasvaara has similar characteristics to those from the undeformed IOCG deposits. Overall the REE patterns suggest a similar REE source for the Fe-oxide–apatite deposits and the non-NDZ Cu–Au deposits (Fig. 16). Both the granitoid suites and intermediate to acid host rocks for the deposits are relatively LREE enriched (e.g. Blake, 1990; Lundmark *et al.*, 2005; Wanhainen *et al.*, 2006), and hence REE could have been derived either from the granitoids or from the intermediate to acid volcanic rocks of the district. The highly saline characteristics of mineralizing fluids in the IOCG deposits (e.g. Lindblom *et al.*, 1996) and the evidence from apatite composition for a lower HF activity in these fluids relative to the Fe oxide–apatite deposit related fluids means that Cl-complexes are likely to have dominated aqueous REE species. Chloride complexation would have had only a minor fractionating effect on REE patterns during extraction from a source rock (Haas *et al.*, 1995), without enhancing Y solubility relative to Dy and Ho.

Titanites from the NDZ hosted deposits are markedly depleted in the LREE relative to the other deposits studied. This could be consistent either with co-precipitation of a particularly LREE-enriched phase, or with alteration subsequently resulting in either leaching of the REE or the partial replacement of titanite by LREE-enriched

phases (see Harlov *et al.*, 2002). However, REE mineral inclusions are absent in Nautanen titanite. Allanite from the same samples is also LREE-depleted relative to other deposit types. In this instance an alternative source for the REE is likely. Gabbro and diorite of both the Haparanda and Perthite-monzonite suites are common in the Nautanen to Aitik area, and the synform marginal to the NDZ at Nautanen is cored by metabasalt of the Porphyrite Group (Bergman *et al.*, 2001). Such an interpretation is supported by the elevated Ni and low Th contents of the Nautanen and Aitik titanites.

Implications for IOCG-type mineralization

The tectonic environment of IOCG mineralization is variable. Hitzman (2000) suggested that IOCG-type mineralization could be linked to cratonic or continental margin environments, associated with orogenic collapse, anorogenic magmatism and subduction, whereas Barton & Johnson (1996) included arc systems, failed continental rifts and active rifts, and stable platforms associated with hotspot volcanism, but noted a suggestion of anorogenic or rift-related origin. This study, linked with previous work on the Norrbotten Fe oxide and IOCG district, demonstrates that both magnetite–apatite deposits and IOCG-type deposits were generated relatively early in the Svecofennian tectonic cycle during subduction and accretion, but either they were modified or there were repeated periods of mineralization through collision to orogenic collapse (Fig. 17). The geochronological data presented here are not consistent with the interpretation of the magnetite–apatite bodies forming as melts consanguinous with their host volcanic rocks, with temporally continuous, hydrothermal modification (Lundberg & Smellie, 1979; Nyström, 1985). The clear inference of an epigenetic origin for the main phase of magnetite–apatite orebody formation and the anomalies introduced into the REE patterns by the effects of aqueous complex formation all argue for a hydrothermal metasomatic origin.

Initial IOCG and Fe oxide–apatite mineralization was temporally associated with Haparanda and Perthite-monzonite suite calc-alkaline magmatism. Subsequent mineralization in post-1800 Ma IOCGs, associated with major deformation zones, has LREE-depleted trace element patterns, suggesting either redistribution of trace elements during metamorphism or a source for the REE and possibly other metals in the volcanic rocks of the region. Preliminary dating from a single sample of regional scapolite–albite altered rock suggests that regional alteration occurred within the period 1912–1895 Ma, corresponding to the initial phase of Fe oxide–apatite mineralization. However, more extensive studies of this alteration are a clear prerequisite for further development of this interpretation.

Models for IOCG mineralization are variable, but many researchers now agree that regional or large-scale albitization or scapolitization released metals to the hydrothermal fluid, resulting in subsequent mineralization in both barren and Cu–Au mineralized magnetite/hematite–apatite ironstones (e.g. Barton & Johnson, 2000; Oliver *et al.*, 2004). The ultimate source of the fluids is currently a matter of debate, as different tracer techniques indicate a wide range of fluid component sources. Pollard (2006) proposed that separation of a fluid phase from calc-alkaline magmas at greater depths than seen in porphyry Cu systems, as a result of higher CO_2 contents, resulted in the circulation of brines along major tectonic structures. Conversely, Barton & Johnson (1996, 2000) pointed to a range of geochemical features favouring non-magmatic brines, sourced from either saline surface waters or the interaction of fluids with evaporites, and developed mass-balance arguments suggesting that magmatic fluids could not be responsible for the scale of regional Na-alteration. The data presented here could be consistent with either model, or indicate different sources of fluid components during the extended and geologically complex history of the deposits. The geochronological data are consistent with a separation in time between Fe oxide–apatite and sulphide mineralization, followed by subsequent alteration of the ores during structurally focused metamorphic fluid flow, whereas the trace element data suggest leaching of metals from both the metavolcanic sequence and the regional granitoids. Meta-evaporite units have been inferred in the Greenstone Group sequence (Frietsch *et al.*, 1997) and hence highly saline non-magmatic brines cannot be excluded from models on the basis of the data presented here. On the basis of high mineralization temperatures and the oxygen isotope composition of quartz, Lindblom *et al.* (1996) favoured a magmatic fluid source at Pahtohavare. Frietsch *et al.* (1995) concluded that sulfur in a range of deposits was derived from both bacterial sulfate reduction and magmatic sources. At present we favour models of hydrothermal genesis for both Fe-oxide and Cu–Au deposits, with Cu–Au mineralization post-dating and overprinting Fe-mineralization, and some metal components of the fluids being derived from local granitoid rocks. The ultimate source of the fluids and dissolved components is yet to be fully constrained.

CONCLUSIONS

The application of spatially constrained LA-ICP-MS to U–Pb analysis has, for the first time, clearly indicated the multistage evolution of titanite from a range of settings in the Norrbotten District, Northern Sweden. The age of the volcanic sequence hosting several major ore deposits and many prospects has been demonstrated to be greater than 2050 Ma and a product of magmatism pre-dating the Svecokarelian orogeny. The iron oxide–apatite deposits,

for which the region is famous, formed in the period 1920–1860 Ma, overlapping with preliminary constraints on the age of regional sodic alteration, although further data on the timing of alteration are necessary to confirm this. An initial phase of iron oxide–copper–gold (IOCG) mineralization temporally overlaps with later stages of this process, within the errors of the data presented here, and corresponds to the 1880–1860 Ma phase of mineralization identified by Billström & Martinsson (2000). Many deposits yield titanite U–Pb ages as late as 1820 and 1790 Ma, but strong evidence of lead loss either by dissolution–reprecipitation or possibly by diffusion suggests that U–Pb ages in this range may represent metamorphism during subsequent thermal events during the Svecokarelian orogeny. Well-constrained, concordant ages in the range 1800–1750 Ma have been obtained from titanite from the Nautanen prospect. Coupled with previous data from the Aitik deposit (Wanhainen *et al.*, 2005) this suggests significant reworking of the initial phase of mineralization alongside further fluid flow episodes along major structural features. The strongly deformed deposits at Malmberget give U–Pb ages extending along concordia over the whole time period and indicate either strong metamorphism at ~1750 Ma or repeated thermal events causing Pb loss from titanite over the whole orogenic cycle.

The trace element chemistry of the analysed titanite is distinct for all the phases of mineralization described above. The LREE-enriched nature of the titanites suggests a metal source either in the intermediate to acid host rocks or in the Svecofennian granitoids of the Haparanda and Perthite-monzonite suites. Minor features of the trace element patterns, such as Y anomalies relative to Dy and Ho, are consistent with a hydrothermal origin for all the titanites studied. Trace element patterns from the Nautanen prospect and Aitik are markedly LREE depleted and may be consistent with a more local trace element source via leaching of metals during alteration of meta-volcanic rocks, or loss of the LREE during metamorphic recrystallization.

Overall the data presented here are consistent with emerging models of IOCG-type mineralization during subduction and continental accretion whereby fluids are channelled along major crustal structures, resulting in regionally extensive alteration, and mineralization focused in structurally controlled fluid discharge zones. The ultimate source of such fluids is not constrained by this study. Different mechanisms and different fluid sources may have operated at different times, as there is a distinction in age between Fe oxide–apatite deposits and sulphide-related Cu–Au mineralization. However, on the basis of current constraints, iron oxide–apatite deposits show some overlap in time with IOCG mineralization, and hence they may have some commonalities in the mechanism of deposit genesis.

ACKNOWLEDGEMENTS

We would like to thank Olaf Martinsson for advice on sampling sites. At the Natural History Museum, London, Anton Kearsley and John Spratt provided assistance with SEM imaging and electron microprobe analyses, Raquel Garcia-Sanchez helped with trace element analysis and Tony Wighton carried out sample preparation. The staff of the Sveriges Geologiska Undersökning office, Malå, Sweden, provided great help in access to drill core and archive data. We would also like to thank Anglo American PLC and Lundin Mining Ltd for permission to work on material from Rakkurijärvi. Referees' comments from Mark Barton and John Hanchar, and editorial comments from Rieto Gieré helped greatly to improve the manuscript.

FUNDING

European Union Regional Development Fund Georange Program Grant 89121.

SUPPLEMENTARY DATA

Supplementary data for this paper are available at *Journal of Petrology* online.

REFERENCES

Barton, M. D. & Johnson, D. A. (1996). Evaporitic-source model for igneous-related Fe oxide-(REE-Cu-Au-U) mineralization. *Geology* **24**, 259–262.

Barton, M. D. & Johnson, D. A. (2000). Alternative brine sources for Fe-oxide(−Cu−Au) systems: Implications for hydrothermal alteration and metals. In: Porter, T. M. (ed.) *Hydrothermal Iron Oxide Copper–Gold and Related Deposits: A Global Perspective*. Adelaide: Australian Mineral Foundation, pp. 43–60.

Bau, M. (1996). Controls on the fractionation of isovalent trace elements in magmatic and aqueous systems: Evidence from Y/Ho, Zr/Hf, and lanthanide tetrad effect. *Contributions to Mineralogy and Petrology* **123**, 323–333.

Bergman, S., Kübler, L. & Martinsson, O. (2001). *Description of regional geological and geophysical maps of northern Norrbotten county*. Stockholm: Sveriges Geologiska Undersökning, Ba 56.

Billström, K. & Martinsson, O. (2000). Links between epigenetic Cu–Au mineralizations and magmatism/deformation in the Norrbotten county, Sweden. In: Weihed, P. and Martinsson, O. (eds) *2nd GEODE Fennoscandian Shield Field Workshop on Palaeoproterozoic and Archaean Greenstone Belts and VMS Districts in the Fennoscandian Shield*. Luleå University of Technology, Research Report **2000:06**, 6.

Blake, K. (1990). The petrology, geochemistry and association to ore formation of the host rocks of the Kiirunavaara magnetite–apatite deposit, northern Sweden. PhD thesis, University of Wales, Cardiff.

Bodnar, R. J. (1994). Synthetic fluid inclusions: XII. The system H_2O–NaCl. Experimental determination of the halite liquidus and isochores for a 40 wt % NaCl solution. *Geochimica et Cosmochimica Acta* **58**, 1053–1063.

Bookstrom, A. (1995). Magmatic features of iron ores of the Kiruna type in Chile and Sweden: ore textures and magnetite geochemistry—A discussion. *Economic Geology* **90**, 469–475.

Broman, C. & Martinsson, O. (2000). Fluid inclusions associated with Cu–Au mineralization in Norrbotten, Sweden. In: Weihed, P. and Martinsson, O. (eds) *2nd GEODE Fennoscandian Shield Field Workshop on Palaeoproterozoic and Archaen Greenstone Belts and VMS Districts in the Fennoscandian Shield*. Luleå University of Technology, Research Report **2000:06**, 7.

Broman, C., Nyström, J. O., Henriquez, F. & Elfman, M. (1999). Fluid inclusions in magnetite–apatite ore from a cooling magmatic system at El Laco, Chile. *GFF* **121**, 253–267.

Carlon, C. J. (2000). Iron oxide systems and base metal mineralisation in northern Sweden. In: Porter, T. M. (ed.) *Hydrothermal Iron Oxide Copper-Gold and Related Deposits: A Global Perspective*. Adelaide: Australian Mineral Foundation, pp. 283–296.

Cherniak, D.J. (1993). Lead diffusion in titanite and preliminary results on the effects of radiation-damage on Pb transport. *Chemical Geology* **110**, 177–194.

Cherniak, D. J. (1995). Sr and Nd diffusion in titanite. *Chemical Geology* **125**, 219–232.

Cliff, R. A. & Rickard, D. (1992). Isotope systematics of the Kiruna magnetite ores, Sweden: Part 2. Evidence for a secondary event 400 m.y. after ore formation. *Economic Geology* **87**, 1121–1129.

Cliff, R. A., Rickard, D. & Blake, K. (1990). Isotope systematics of the Kiruna magnetite ores, Sweden: Part 1. Age of the ore. *Economic Geology* **85**, 1770–1776.

Edfelt, Å., Armstrong, R. N., Smith, M. P. & Martinsson, O. (2005). Alteration paragenesis and mineral chemistry of the Tjårrojåkka apatite–iron and Cu (–Au) occurrences, Kiruna area, northern Sweden. *Mineralium Deposita* **40**, 409–434.

Edfelt, Å., Smith, M. P., Armstrong, R. N. & Martinsson, O. (2007). Apatite chemistry—applications for characterising apatite–iron and IOCG deposits. Paper IV. In: Edfelt, Å. *The Tjårrojåkka apatite–iron and Cu (–Au) deposits, northern Sweden: products of one ore forming event*. PhD thesis, Luleå University of Technology.

Ekdahl, E. (1993). Early Proterozoic Karelian and Svecofennian formations and evolution of the Raahe–Ladoga ore zone, based on the Pielavesi area, central Finland. *Geological Survey of Finland Bulletin* **373**, 1–137.

Frietsch, R. & Perdahl, J.-A. (1995). Rare earth elements in apatite and magnetite in Kiruna-type iron ores and some other iron ore types. *Ore Geology Reviews* **9**, 489–510.

Frietsch, R., Billström, K. & Perdahl, J.-A. (1995). Sulphur isotopes in Lower Proterozoic iron and sulphide ores in northern Sweden. *Mineralium Deposita* **30**, 275–284.

Frietsch, R., Tuisku, P., Martinsson, O. & Perdahl, J.-A. (1997). Early Proterozoic Cu–(Au) and Fe ore deposits associated with regional Na–Cl metasomatism in northern Fennoscandia. *Ore Geology Reviews* **12**, 1–34.

Frost, B. R., Chamberlain, K. R., Schumacher, J. C., Scott, D. J. & Moser, D. E. (2000). Sphene (titanite); phase relations and role as a geochronometer. *Chemical Geology* **172**, 131–148.

Gagnon, J. R., Samson, I. M., Fryer, B. J. & Williams-Jones, A. E. (2004). The composition and origin of hydrothermal fluids in a NYF-type granitic pegmatite, South Platte District, Colorado: evidence from LA-ICP-MS analysis of fluorite and quartz-hosted fluid inclusions. *Canadian Mineralogist* **42**, 1331–1355.

Gieré, R. (1986). Zirconolite, allanite and hoegbomite in a marble skarn from the Bergell contact aureole—implications for mobility of Ti, Zr and REE. *Contributions to Mineralogy and Petrology* **93**, 459–470.

Gieré, R. (1990). Hydrothermal mobility of Ti, Zr and REE: examples from the Bergell and Adamello contact aureoles (Italy). *Terra Nova* **2**, 60–67.

Geijer, P. (1910). Igneous rocks and iron ores of Kiirunavaara, Luossavaara and Tuolluvaara. *Scientific and Practical Researches in Lapland Arranged by Luossavaara–Kiirunavaara Aktiebolag, Stockholm*.

Geijer, P. (1931). Berggrunden inom malmtrakten Kiruna–Gallivare–Pajala. *Sveriges Geologiska Undersökning, Series C*, 366.

Haas, J. R., Shock, E. S. & Sassani, D. C. (1995). Rare-earth elements in hydrothermal systems—estimates of standard partial molal thermodynamic properties of aqueous complexes of the rare-earth elements at high-pressures and temperatures. *Geochimica et Cosmochimica Acta* **59**, 4329–4350.

Harlov, D. E., Andersson, U. B., Forster, H. J., Nyström, J. O., Dulski, P. & Broman, C. (2002). Apatite–monazite relations in the Kiirunavaara magnetite–apatite ore, northern Sweden. *Chemical Geology* **191**, 47–72.

Henderson, P. (1980). Rare earth element partition between sphene, apatite and other coexisting minerals of the Kangerdlugssuaq intrusion, E. Greenland. *Contributions to Mineralogy and Petrology* **72**, 81–85.

Hitzman, M. (2000). Iron oxide–Cu–Au deposits: what, where, when, and why? In: Porter, T. M. (ed.) *Hydrothermal Iron Oxide Copper–Gold and Related Deposits: A Global Perspective*. Adelaide, Australian Mineral Foundation, pp. 9–20.

Hitzman, M., Oreskes, N. & Einaudi, M. T. (1992). Geological characteristics and tectonic setting of Proterozoic iron oxide (Cu–U–Au–REE) deposits. *Precambrian Research* **58**, 241–287.

Jeffries, T. E. (2004). Laser ablation inductively plasma mass spectrometry. In: Janssens, K. & Van Grieken, R. (eds) *Comprehensive Analytical Chemistry XLII. Non-Destructive Microanalysis of Cultural Heritage Materials*. Amsterdam: Elsevier, pp. 313–358.

Jochum, K. P., Nohl, U., Herwig, K., Lammel, E., Stoll, B. & Hofmann, A. W. (2005). GeoReM: a new geochemical database for reference materials and isotopic standards. *Geostandards and Geoanalytical Research* **29**, 333–338.

Korzhinskiy, M. A. (1981). Apatite solid solutions as indicators of the fugacity of HCl and HF in hydrothermal fluids. *Geochemistry International* **3**, 45–60.

Lahtinen, R., Huhma, H. & Kousa, J. (2002). Contrasting source components of the Paleoproterozoic Svecofennian metasediments: Detrital zircon U–Pb, Sm–Nd and geochemical data. *Precambrian Research* **116**, 81–109.

Lindblom, S., Broman, C. & Martinsson, O. (1996). Magmatic–hydrothermal fluids in the Pahtohavare Cu–Au deposit in greenstone at Kiruna, Sweden. *Mineralium Deposita* **31**, 307–318.

Ludwig, K. R. (2003). *User's manual for Isoplot 3.00 a geochronological toolkit for Microsoft Excel. Berkeley Geochronology Center Special Publication* **4**.

Lundberg, B. & Smellie, J. A. T. (1979). Painrova and Mertainen: two deposits of the Kiruna iron ore type in northern Sweden. *Economic Geology* **74**, 1131–1152.

Lundmark, C., Billström, K. & Weihed, P. (2005). The Jokkmokk granitoid, an example of 1·88 Ga juvenile magmatism at the Archaean–Proterozoic border in northern Sweden. *GFF* **127**, 83–98.

McIntire, W. L. (1963). Trace element partition coefficients—a review of theory and applications to geology. *Geochimica et Cosmochimica Acta* **27**, 1209–1264.

Martinsson, O. (1997). Tectonic setting and Metallogeny of the Kiruna Greenstones. Doctoral thesis, Luleå University of Technology.

Martinsson, O. (2004). Geology and Metallogeny of the Northern Norrbotten Fe–Cu–Au Province. In: Allen, R. L., Martinsson, O.

& Weihed, P. (eds) *Svecofennian Ore-Forming Environments: Volcanic-Associated Zn-Cu-Au-Ag, Intrusion-Associated Cu-Au, Sediment-Hosted Pb-Zn, and Magnetite-Apatite Deposits of Northern Sweden, Society of Economic Geologists Guidebook Series* **33**, 131–148.

Martinsson, O. & Virkkunen, R. (2004). Apatite Iron Ores in the Gällivare, Svappavaara, and Jukkasjärvi Areas. In: Allen, R. L., Martinsson, O. & Weihed, P. (eds) *Svecofennian Ore-Forming Environments: Volcanic-Associated Zn-Cu-Au-Ag, Intrusion-Associated Cu-Au, Sediment-Hosted Pb-Zn, and Magnetite-Apatite Deposits of Northern Sweden, Society of Economic Geologists Guidebook Series* **33**, 167–172.

Martinsson, O. & Wanhainen, C. (2000). Excursion guide. In: Weihed, P. & Martisson, O. (eds) *2nd GEODE Fennoscandian Shield Field Workshop on Palaeoproterozoic and Archaen Greenstone Belts and VMS Districts in the Fennocandian Shield* **2000:6**, 63–76.

Martinsson, O. & Wanhainen, C. (2004). Character of Cu–Au Mineralization and Related Hydrothermal Alteration along the Nautanen Deformation Zone, Gällivare Area, Northern Sweden. In: Allen, R. L., Martinsson, O. & Weihed, P. (eds) *Svecofennian Ore-Forming Environments: Volcanic-Associated Zn-Cu-Au-Ag, Intrusion-Associated Cu-Au, Sediment-Hosted Pb-Zn, and Magnetite-Apatite Deposits of Northern Sweden, Society of Economic Geologists Guidebook Series* **33**, 149–160.

Möller, P. (1998). Rare earth elements and yttrium fractionation caused by fluid migration. In: Novák, M. & Rosenbaum, J. (eds) *Challenges to Chemical Geology. Referenced Papers from MAEGS-10.* Czech Geological Survey, Prague, pp. 9–32.

Naslund, H. R., Henriquez, F., Nyström, J. O., Vivallo, W. & Dobbs, F. M. (2002). Magmatic iron ores and associated mineralisation: examples from the Chilean high Andes and coastal Cordillera. In: Porter, T. M. (ed.) *Hydrothermal Iron Oxide Copper–Gold and Related Deposits; A Global Perspective, 2.* Adelaide: PGC Publishing, pp. 207–226.

Nironen, M. (1997). The Svecofennian Orogen: a tectonic model. *Precambrian Research* **86**, 21–44.

Norman, M. D., Griffin, W. L., Pearson, N. J., Garcia, M. O. & O'Reilly, S. Y. (1998). Quantitative analysis of trace element abundances in glasses and minerals: a comparison of laser ablation inductively coupled plasma mass spectrometry, solution inductively coupled plasma mass spectrometry, proton microprobe and electron microprobe data. *Journal of Analytical Atomic Spectrometry* **13**, 477–482.

Nyström, J. O. (1985). Apatite iron ores of the Kiruna field, northern Sweden: magmatic textures and carbonatitic affinity. *GFF* **107**, 133–141.

Nyström, J. O. & Henríquez, F. (1994). Magmatic features of iron of the Kiruna type in Chile and Sweden: ore textures and magnetite geochemistry. *Economic Geology* **89**, 820–839.

Oliver, N. H. S., Cleverley, J. S., Mark, G., Pollard, P. J., Bin Fu, , Marshall, L. J., Rubenach, M. J., Williams, P. J. & Baker, T. (2004). Modeling the role of sodic alteration in the genesis of iron oxide–copper–gold deposits, eastern Mount Isa block, Australia. *Economic Geology* **99**, 1145–1176.

Oreskes, N., Rhodes, A. L., Sheets, S. A. & Espinoza, S. (1995). Evidence for formation of magnetite by hydrothermal processes at El Laco, Chile, Part 1: Field relations and alteration assemblages. *Geological Society of America, Abstracts with Programs* **27**, A467.

Parak, T. (1975). Kiruna iron ores are not 'intrusive magmatic ores of the Kiruna type'. *Economic Geology* **70**, 1242–1258.

Petrik, I., Broska, I., Lipka, J. & Siman, P. (1995). Granitoid allanite-(Ce): substitution relations, redox conditions and REE distribution in an example of I-type granitoids, western Carpathians, Slovakia. *Geologica Carpathica* **46**, 79–94.

Pollard, P. J. (2006). An intrusion-related origin for Cu–Au mineralization in iron oxide–copper–gold (IOGG) provinces. *Mineralium Deposita* **41**, 179–187.

Prowatke, S. & Klemme, S. (2005). Effect of melt composition on the partitioning of trace elements between titanite and silicate melt. *Geochimica et Cosmochimica Acta* **69**, 695–709.

Putnis, A. (2002). Mineral replacement reactions: from macroscopic observations to microscopic mechanisms. *Mineralogical Magazine* **66**, 689–708.

Ribbe, P. H. (1980). Titanite. In: Ribbe, P. H. (ed.) *Orthosilicates. Mineralogical Society of America, Reviews in Mineralogy and Geochemistry* **5**, 137–154.

Romer, R. L., Kjösnes, B., Korneliussen, A., Lindahl, I., Skysseth, T., Standal, H. & Sundvoll, B. (1992). The Archaean–Proterozoic boundary beneath the Caledonides of northern Norway and Sweden: U–Pb, Rb–Sr and Nd isotopic data from the Rombak–Tysfjord area. *Norges Geologiske Undersøkelse, Rapport* **91**.

Romer, R. L., Martinsson, O. & Perdahl, J.-A. (1994). Geochronology of the Kiruna iron ores and hydrothermal alteration. *Economic Geology* **89**, 1249–1261.

Romer, R., Martinsson, O. & Perdahl, J.-A. (1996). Scapolite: A tracer for the initial lead isotopic composition in sulfide deposits with later additions of radiogenic lead. *Mineralium Deposita* **31**, 134–139.

Rubin, J. N., Henry, C. D. & Price, J. G. (1993). The mobility of zirconium and other 'immobile' elements during hydrothermal alteration. *Chemical Geology* **110**, 29–47.

Salvi, S. & Williams-Jones, A. E. (1990). the role of hydrothermal processes in the granite-hosted Zr, Y, REE deposit at Strange Lake, Quebec, Labrador—evidence from fluid inclusions. *Geochimica et Cosmochimica Acta* **54**, 2403–2418.

Salvi, S. & Williams-Jones, A. E. (1996). The role of hydrothermal processes in concentrating high-field strength elements in the Strange Lake peralkaline complex, northeastern Canada. *Geochimica et Cosmochimica Acta* **60**, 1917–1932.

Shannon, R. D. (1976). Revised Effective Ionic Radii and Systematic Studies of Interatomic Distances in Halides and Chaleogenides. *Acta Crystallographica* **A32**, 751–767.

Sillitoe, R. H. (2003). Iron oxide–copper–gold deposits: an Andean view. *Mineralium Deposita* **38**, 787–812.

Skiöld, T. (1987). Aspects of the Proterozoic geochronology of Northern Sweden. *Precambrian Research* **35**, 161–167.

Skiöld, T. (1988). Implications of new U–Pb zircon chronology to early Proterozoic crustal accretion in northern Sweden. *Precambrian Research* **32**, 35–44.

Skiöld, T. & Cliff, R. A. (1984). Sm–Nd and U–Pb dating of early Proterozoic mafic–felsic volcanism in northernmost Sweden. *Precambrian Research* **26**, 1–13.

Smith, M. P. (2007). Metasomatic silicate chemistry at the Bayan Obo Fe–REE–Nb deposit, Inner Mongolia, China: Contrasting chemistry and evolution of fenitising and mineralising fluids. *Lithos* **93**, 126–148.

Smith, M. P. & Gleeson, S. A. (2005). Constraints on the source and evolution of mineralising fluids in the Norrbotten, Fe oxide–Cu–Au province, Sweden. *Mineral Deposits Research: Meeting the Global Challenge: Proceedings of the Eighth Biennial SGA Meeting, Beijing, China, 18–21 August 2005.* Berlin: Springer pp. 825–828.

Smith, M. P., Coppard, J., Herrington, R. & Stein, H. (2007). The geology of the Rakkurijärvi Cu–(Au) prospect, Norrbotten: A new IOCG deposit in Northern Sweden. *Economic Geology* **102**, 393–414.

Smith, R. J. (2002). Geophysics of iron oxide copper–gold deposits. In: Porter, T. M. (ed.) *Hydrothermal Iron Oxide Copper–Gold and Related*

Deposits; A Global Perspective, 2. Adelaide: PGC Publishing, pp. 357–367.

Stacey, J. S. & Kramers, J. D. (1975). Approximation of terrestrial lead isotope evolution by a two-stage model. *Earth and Planetary Science Letters* **26**, 207–221.

Storey, C. D., Jeffries, T. E. & Smith, M. (2006). Common lead corrected laser ablation ICP-MS systematics and geochronology of titanite. *Chemical Geology* **227**, 37–52.

Storey, C. D., Smith, M. P. & Jeffries, T. E. (2007). *In situ* LA-ICP-MS U–Pb dating of metavolcanics of Norrbotten, Sweden: Records of extended geological histories in complex titanite grains. *Chemical Geology* **240**, 163–181.

Sveriges Geologiska Undersökning (1967). *Berggrundsgeologiska och flygmagnetiska kartbladen Kiruna NV, NO, SV, SO*. Stockholm: Sveriges Geologiska Undersökning (map).

Tiepolo, M., Oberti, R. & Vannucci, R. (2002). Trace-element incorporation in titanite: constraints from experimentally determined solid/liquid partition coefficients. *Chemical Geology* **191**, 105–119.

Tomaschek, F., Kennedy, A. K., Villa, I. M., Lagos, M. & Ballhaus, C. (2003). Zircons from Syros, Cyclades, Greece—Recrystallization and mobilization of zircon during high-pressure metamorphism. *Journal of Petrology* **44**, 1977–2002.

Vityk, M. O. (1995). Do fluid inclusions in high-grade metamorphic terranes preserve peak metamorphic density during retrograde decompression? *American Mineralogist* **80**, 641–644.

Wägman, K. & Ohlsson, L.-G. (2000). *Exploration opportunities in Norrbotten: Municipality of Kiruna*. Stockholm: Mineral Resources Information Office, Sveriges Geologiska Undersökning, 278 pp.

Wakita, H., Rey, P. & Schmidt, R. A. (1971). Abundances of the 14 rare-earth elements and 12 other trace elements in Apollo 12 samples: Five igneous and one breccia rocks and four soils. *Proceedings of the Second Lunar Science Conference. Geochimica et Cosmochimica Acta Supplement* **2**, 1319–1329.

Wanhainen, C., Broman, C. & Martinsson, O. (2003). The Aitik Cu–Au–Ag deposit in northern Sweden: a product of high salinity fluids. *Mineralium Deposita* **38**, 715–726.

Wanhainen, C., Billström, K., Martinsson, O., Stein, H. & Nordin, R. (2005). 160 Ma of magmatic/hydrothermal and metamorphic activity in the Gallivare area: Re–Os dating of molybdenite and U–Pb dating of titanite from the Aitik Cu–Au–Ag deposit, northern Sweden. *Mineralium Deposita* **40**, 435–447.

Wanhainen, C., Billström, K. & Martinsson, O. (2006). Age, petrology and geochemistry of the porphyritic Aitik intrusion, and its relation to the disseminated Aitik Cu–Au–Ag deposit, northern Sweden. *GFF* **128**, 273–286.

Weihed, P., Arndt, N., Billström, K., Duchesne, J. C., Eilu, P., Martinsson, O., Papunen, H. & Lahtinen, R. (2005). Precambrian geodynamics and ore formation: The Fennoscandian Shield. *Ore Geology Reviews* **27**, 273–322.

Welin, E. (1987). The depositional evolution of the Svecofennian supracrustal sequence in Finland and Sweden. *Precambrian Research* **35**, 95–113.

Wiedenbeck, M., Alle, P., Corfu, F., Griffin, W. L., Meier, M., Oberli, F., Vonquadt, A., Roddick, J. C. & Speigel, W. (1995). 3 Natural Zircon Standards for U–Th–Pb, Lu–Hf, Trace-Element and REE Analyses. *Geostandards Newsletter* **19**, 1–23.

Williams, C. T. (1996). Analysis of rare earth minerals. In: Jones, A. P., Wall, F. & Williams, C. T. (eds) *Rare Earth Minerals: Chemistry, Origin and Ore Deposits*. London: Chapman & Hall, pp. 327–348.

Williams, I. S. (1998). U–Th–Pb geochronology by ion microprobe. In: McKibben, M. A., Shanks, W. C., , III & Ridley, W. I. (eds) *Applications of Microanalytical Techniques to Understanding Mineralizing processes. Reviews in Economic Geology* **7**, 1–35.

Williams, P. J., Barton, M. D., Johnson, D. A., Fontbote, L., de Haller, A., Mark, G., Oliver, N. H. S. & Marschik, R. (2000). Iron oxide copper gold deposits; geology, space–time distribution, and possible modes of origin? In: Hedenquist, J. W., Goldfarb, R. J. & Richards, J. P. (eds) *Society of Economic Geologists, USA*, pp. 371–405.

Witschard, F. (1984). The geological and tectonic evolution of the Precambrian of northern Sweden—a case for basement reactivation? *Precambrian Research* **23**, 273–315.